energies

MDPI

Article

# Framework for Energy-Averaged Emission Mitigation Technique Adopting Gasoline-Methanol Blend Replacement and Piston Design Exchange

**Prakash Chandra Mishra [1,*], Anand Gupta [2], Saikat Samanta [3], Rihana B. Ishaq [4] and Fuad Khoshnaw [5]**

1 Department of Mechanical Engineering, Veer Surendra Sai University of Technology, Burla 768018, India
2 Department of Mechanical Engineering, Indira Gandhi Institute of Technology, Sarang 759146, India
3 School of Mechanical Engineering, KIIT University, Bhubaneswar 751024, India
4 School of Built Environment Engineering and Computing, Leeds Beckett University, Leeds LS1 3HE, UK
5 School of Engineering and Sustainable Development, De Montfort University, Leicester LE1 9BH, UK
* Correspondence: pcmishra_me@vssut.ac.in; Tel.: +91-8917535445

**Abstract:** Measurement to mitigate automotive emission varies from energy content modification of fuel to waste energy recovery through energy system upgradation. The proposed energy-averaged emission mitigation technique involves interfacing piston design exchange and gasoline–methanol blend replacement with traditional gasoline for low carbon high energy content creation. Here, we interlinked the CO, $CO_2$, $NO_x$, $O_2$, and HC to different design exchanges of coated pistons through the available brake power and speed of the engine. We assessed the relative effectiveness of various designs and coating thicknesses for different gasoline–methanol blends (0%,5%,10%, and 15%). The analysis shows the replacement of 5%, 10%, and 15% by volume of gasoline with methanol reduces the fuel carbon by 4.167%, 8.34%, and 12.5%, respectively. The fuel characteristics of blends are comparable to gasoline, hence there is no energy infrastructure modification required to develop the same amount of power. The CO and HC reduced significantly, while $CO_2$ and $NO_x$ emissions are comparable. Increasing the coating thickness enhances the surface temperature retention and reduces heat transfer. The Type_C design of the steel piston and type_A design of the AlSi piston show temperature retention values of 582 °C and 598 °C, respectively. Type_A and type_B pistons are better compared to type_C and the type_D piston design for emission mitigation due to decarbonization of fuel through gasoline-methanol blend replacement. Surface response methodology predicts Delastic, σvon Mises, and Tsurface with percentage errors of 0.0042,0.35, and 0.9, respectively.

**Keywords:** energy-averaged emission mitigation; gasoline-methanol blend; piston design exchange; fuel carbon reduction

check for updates

**Citation:** Mishra, P.C.; Gupta, A.; Samanta, S.; Ishaq, R.B.; Khoshnaw, F. Framework for Energy-Averaged Emission Mitigation Technique Adopting Gasoline-Methanol Blend Replacement and Piston Design Exchange. *Energies* **2022**, *15*, 7188. https://doi.org/10.3390/en15197188

Academic Editor: Yonmo Sung

Received: 31 August 2022
Accepted: 25 September 2022
Published: 29 September 2022



## 1. Introduction

An increase in the demand for emission control and stringent regulation [1] for energy usage forces energy investors to switch from high-carbon high-energy sources to low-carbon high-energy sources to meet day-to-day energy demands [2]. Energy-intensive carbon mitigation strategies, such as carbon avoidance, carbon embedding, and carbon removal policies are adopted for the faster control of climate degradation through intelligent energy usage [3]. The simultaneous restructuring of the energy infrastructure [4–6] and energy content modification are highly expensive reformation initiatives in the energy sector [7]. Such decoupling may lead to energy poverty due to the sudden termination of specialty sectors to be replaced with clean and green carbon-negative energy resources [8,9]. The intelligent interconnection of different energy resources in the sequential grid to deal with the high fluctuation of energy mode swing would be a better approach towards the restructuring of the energy infrastructure [10]. Energy decision making in the global transition to a low-carbon, high energy efficiency-based emission mitigation technique

sometimes proves to be extremely costly energy-wise, and adds more expenditure on the global energy budget[11]. An energy innovation strategy with minimum infrastructural reformation and optimum decarbonization [11,12] potential would not trigger much in the way of the social dynamics of energy behavior. It would be a sustainability energy alternative for the near future.

Through the carbon avoidance technique, carbon content at 4.167% ($B_5$), 8.34% ($B_{10}$), and 12.5% ($B_{15}$) could be removed from traditional gasoline fuel through blending to study the emission mitigation potential of the newly formulated fuel [7]. Carbon removal up to 15% through blending [13] hardly affects the energy content of fuel[11]. Moreover, no significant reformation in the energy infrastructure is required. Toxicity, acid value, and corrosion-like redundant effects are not aggressive in these flexi-fuel formations. With higher heat content, a better-quality flash point, pour point, and viscosity are observed, which are comparable or superior to traditional fuels. However, sometimes, due to an increase in the % of methanol, $NO_x$ emission (though it reduces carbonated emissions)formation is aggravated multiple times due to improved combustion [14] and enhanced exhaust muffler temperature [12,15]. Over the years, methanol as IC engine fuel is greatly evaluated [16] and methanol economy in China [17] is investigated with environmental implications. Cleaner production of methanol [18] is highly compatible with the existing industrial infrastructure and hydrogenation and reformation technology [19]. Methanol blending over the total replacement of fuel, especially with gasoline, is found to be successful due to insignificant changes in fuel properties. Without any compromise in energy and efficiency, the carbonated emissions [14], such CO, $CO_2$, and HC, reduced significantly due to the use of blends [20]. However, $NO_x$ emission is a concern regarding the use of blends. Though there are techniques, such as the Miller cycle [21], muffler design modification [22], catalytic reduction [22,23], etc., which are suggested to reduce $NO_x$, an enhanced combustion chamber surface temperature [24,25] necessitates the thermal analysis of engine components with different coatings for different applications. For example, functionally graded coating in AlSi and steel pistons [26] or ceramic-coated pistons, especially for diesel engine [27] application [28], proved to be energy efficient. This is evident from thermal analysis of coated pistons using FEA [29].

Automotive Emission is controlled through multiple upgradation techniques without compromising energy and efficiency of the engine. Through appropriate experimentations, simulation, and optimization [15,30,31], this is proved. However, a simultaneous investigation of blend replacement [32–34] and coated piston design exchange analysis, as well as its effect on the energy and efficiency of the engine through a predicted and actual comparison using response surface methodology (RSM) [35–38],is a step forward andwasthe aim of this investigation. Though there are a limited number of works carried out in the blending of diesel with alcohols [39,40] gasoline–methanol blends and piston design exchange are a further step in this direction. Figure 1a,b show the energy dynamics of engine combustion and the steps for interfacing fuel replacement and piston design exchange.

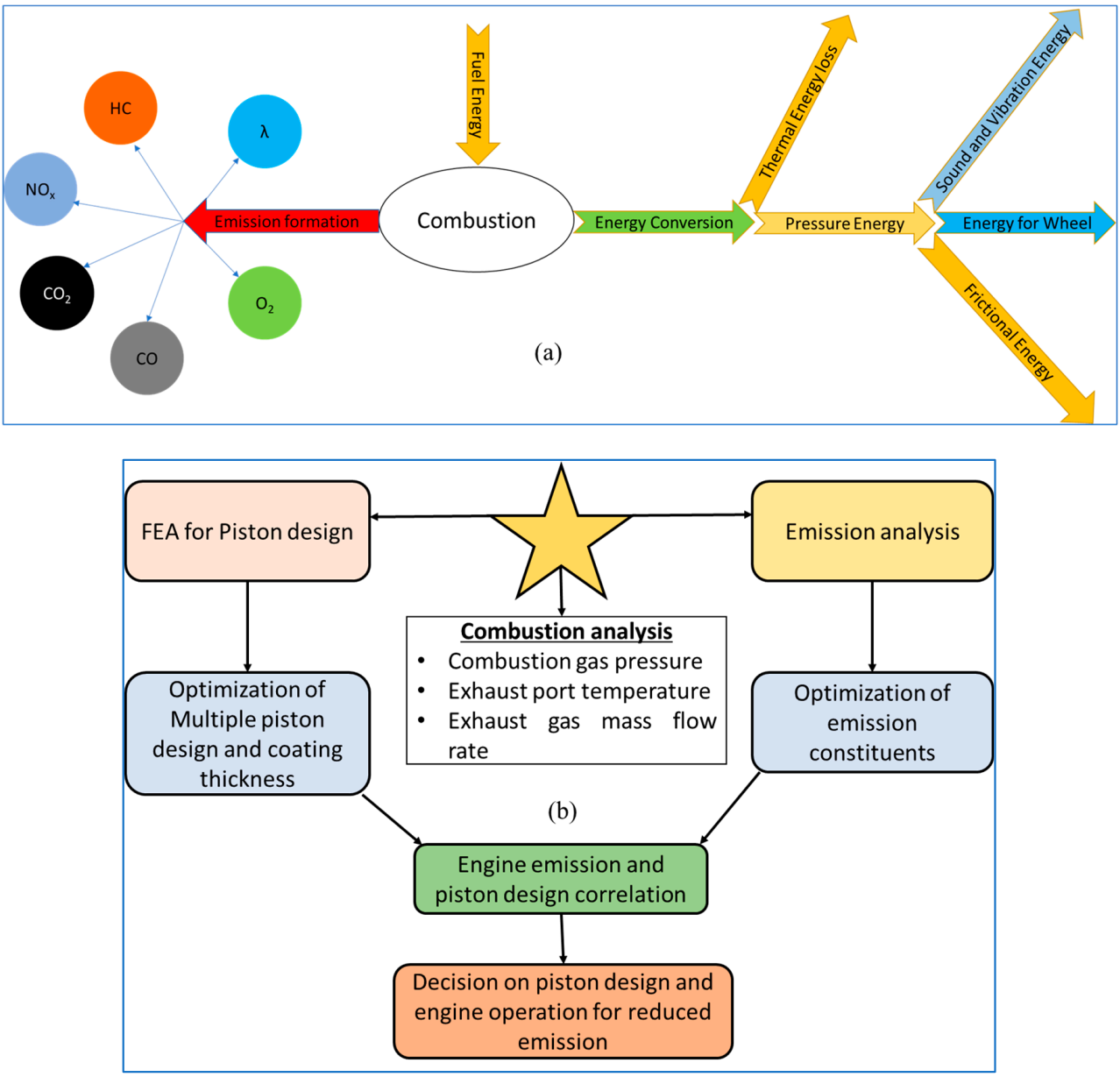


**Figure 1.** Framework for (**a**)energy dynamics of engine system subjected to low-carbon alternatives; (**b**)interfacing of fuel replacement and piston design to mitigate emission and improve energy efficiency.

## 2. Methods

**Fuel carbon reduction through blending and fuel characterization.** Gasoline and methanol were added in different proportions to prepare different blends ($B_5$, $B_{10}$, and $B_{15}$). Such a replacement ensures carbon avoidance. Equations (1)–(3) show the amount of carbon removed through blending.

$$\%\text{ carbon removal }(B_5) = \frac{100 \times 6 - (95 \times 6 + 1 \times 5)}{100 \times 6} = 4.167\% \quad (1)$$

$$\%\text{ carbon removal }(B_{10}) = \frac{100 \times 6 - (90 \times 6 + 1 \times 10)}{100 \times 6} = 8.34\% \quad (2)$$

$$\%\text{ carbon removal }(B_{15}) = \frac{100 \times 6 - (85 \times 6 + 1 \times 15)}{100 \times 6} = 12.5\% \quad (3)$$

To evaluate the formulated fuel characteristics, the ASTM standard procedures were followed. Fuel density (by ASTM 4052), kinetic viscosity (using ASTM D445), acid value (using ASTM D664), flash point (by ASTM D93), calorific value (by ASTM D240), auto-ignition temperature (using ASTM E 659), Octane-MON (using ASTM D2700-MON), and Octane-RON (by ASTM D2700-RON) were measured and are explained in the Results and Discussion section. The modified fuel characteristics of the blends are very close to that of gasoline, hence this alternate arrangement is.

The quantitative equations to estimate different fuel properties is given in Equations (4)–(11). The density of the gasoline and petroleum blend was numerically computed as per Equation (4).

$$\rho_{blend} = \frac{\rho_g \nu_g + \rho_m \nu_m}{\nu_g + \nu_m} \tag{4}$$

There are three different methods to numerically estimate the kinetic viscosity of a gasoline and methanol blend: the Gambill method, the Refuta equation, and the Chevron formula, as given in Equation (5), Equation (6), and Equation (7), respectively.

$$\kappa_{blend} = x_g \kappa_g{}^{\frac{1}{3}} + x_m \kappa_m{}^{\frac{1}{3}} \tag{5}$$

Refuta-mass fraction procedure:

$$VBN_i = 14.534 \times \ln(\ln(\kappa_i + 0.8)) + 10.975 \tag{6}$$

$$VBN_{blend} = \sum_{i=0}^{n=0} x_i VBN_i \tag{7}$$

$$\kappa_{blend} = \exp\left(\exp\left(\frac{VBN_{blend} - 10.975}{14.534}\right)\right) - 0.8 \tag{8}$$

Chevron formula (volumetric basis):

$$VBN_i = \frac{\ln(\kappa_i)}{\ln(1000 \times \kappa_i)} \tag{9}$$

$$VBN_{blend} = \sum_{i=0}^{n=0} v_i VBN_i \tag{10}$$

The octane number of a methanol–gasoline blend is estimated on the basis of the formula given in Equation (11):

$$OCT_{blend} = OCT_{gasoline} \times \left(v_{gasoline}\right) + OCT_{methanol} \times (v_{methanol}) \tag{11}$$

Now, there is the requirement of understanding the fuel characteristics of the newly formulated blended fuel, with a particular emphasis on the comparison to pure gasoline. Figure 2a–d show different piston designs under consideration.

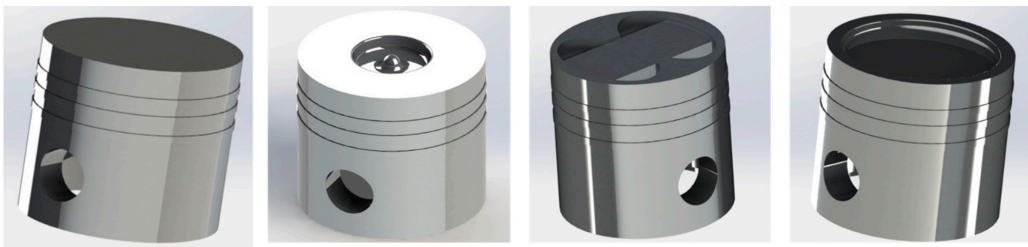

(**a**) (**b**) (**c**) (**d**)

**Figure 2.** Multi piston design consideration: (**a**). Flat head-A; (**b**)-bowl design-B; (**c**)-bowl design-C and; (**d**) bowl design-D.

## 3. Energy Conversion and Emission Measurement

The engine test rig used here was equipped with a single-cylinder four-stroke petrol engine mounted in a universal test bed and coupled with a water-cooled eddy current dynamometer [13]. The engine used here is air-cooled with a cylinder displacement of 105.6 cc, delivering maximum power of 5.59 kW at 7500 rpm and a maximum torque of 7.85 Nm at 6000 rpm at full load condition. Hence, the maximum operational testing torque was fixed to be 5 Nm. The testing targeted 500 rpm, 1000 rpm, and 1500 rpm, while the torque was set to 2 Nm, 3 Nm, 5 Nm, respectively [11]. The equivalent value of the brake mean effective pressure (BMEP) is 2.38 bar, 3.57 bar, and 5.95 bar, respectively. The details of the specification of the engine and dynamometer are given in the Supplementary Materials. The eddy current dynamometer equipped with a APPSYS WED 38S type magnetic water strainer was engaged in this study. It can monitor a maximum engine torque of 90 Nm and a speed of 7000 rpm. Other attachments include a torque calibration arm, water flow switch, magnetic pickup sensor, and reaction type torque sensor. The control panel contains a data acquisition system, computer hardware, and peripheral component interconnect (PCI) data card. The control panel monitors pressure ($N/m^2$), temperature (°C), mechanical power (kW/HP), speed (rpm), and torque (Nm). The data generated from a running engine are saved in Excel form along with various graphical plots. The dynamometer has a control system for either manual or automatic mode. The testing arrangement also includes a six-gas emission analyzer of HORIBA make MEXA-584L, which can simultaneously sense CO, $CO_2$, $NO_x$, lambda, HC, and $O_2$. It uses the non-dispersive infrared (NDIR) technique. The measuring steps in this machine include a leak detection test and an HC hang up test to be passed prior to taking the reading of various combinations of torque (Nm) and speed (Nm) [11]. The data acquisition system attached to the dynamometer ensures the speed and torque at which emission from the engine is recorded. Table 1 shows the list of instruments with a measuring range for experiments.

**Table 1.** List of instruments with measuring range, accuracy, and uncertainty %.

| Measured Quantity | Measurement Range | Accuracy | Type of Instrument | % Uncertainty |
|---|---|---|---|---|
| Load | ±90 Nm | ±0.1 Nm | Strain gauge type load cell | ±0.1 Nm |
| Speed | 0–7000 rpm | ±1 rpm | Magnetic pick-up type speed sensor | ±0.1 rpm |
| Time | - | ±0.1 s | - | ±0.2 s |
| CO | 0–10% by vol | ±0.001% | Non-dispersive infrared gas sensor | ±1 |
| $CO_2$ | 0–20% by vol | ±0.001% | Non-dispersive infrared gas sensor | ±1 |
| $NO_x$ | 0–5000 ppm | ±1 ppm | Electro chemical gas sensor | ±0.6 |
| EGT | 0–900°C | ±0.3 °C | K-type thermo-couple | ±0.1 |

Through emission investigation, the effect of fuel carbon redundancy on various emission constituents at a constant rpm, coating thicknesses, and variable BMEP were investigated. Furthermore, for 1500 rpm, 5.95 bar (BMEP), and variable coating thicknesses, the various emission constituents were measured. Additionally, keeping the rpm to 1500, the BMEP@5.95 bar, and the CT@0.8 mm, emission behavior for the design exchange of the piston was considered to depict the fuel carbon redundant effect. The change in the value of fuel characteristic parameters did not deviate too much from that of the current gasoline. So, replacing $B_5$, $B_{10}$, and $B_{15}$ with gasoline is acceptable. Next, it was required to test the newly formed fuel for energy efficiency and emission formation. Engine testing, emission, and performance measurement procedures are discussed in the Method section. The effect of the piston design exchange and coating thickness is included in the emission, the elastic behavior of the coated and uncoated pistons were achieved through finite element analysis (FEA), and the temperature is validated by Buyukkyaet al. [29] at crown center and bowl rim locations for different coating thicknesses and piston materials (steel, AlSi).

## 4. Emission Formation Mechanism

CO formation: CO is formed in burned gases due to the incomplete oxidation of fuel carbon and the subsequently insufficient oxygen available for the complete oxidation of fuel. If the A/F ratio decreases below the stochiometric A/F ratio, then the CO emission rises.

$CO_2$ formation: There are two steps involved inthe emission formation mechanism of $CO_2$. In the first step, HC is converted to CO. Intermediate molecules, such as HC, aldehyde, and ketones, are formed through many sequential oxidation processes, which is given in Equation (12):

$$\mathrm{RH} \rightarrow \mathrm{R} + \mathrm{O_2} \rightarrow \mathrm{RCHO} \rightarrow \mathrm{RCO} \rightarrow \mathrm{CO} \tag{12}$$

In the second step, CO is converted into $CO_2$ due to the presence of enough oxygen in the air. $CO_2$ formation is only possible due to complete combustion (sufficient time and sufficient oxygen to eliminate unburnt HC). The amount of $CO_2$ emission formed has a direct influence on the engine performance. In the recently developed engine, reduction in $CO_2$ was observed due to an improved combustion process.

$$2\mathrm{CO} + 2\mathrm{OH} \rightarrow 2\mathrm{CO_2} + \mathrm{H_2} \tag{13}$$

$NO_x$ formation: $NO_x$ is formed due to the oxidation of molecular Nitrogen. With elevated flames during combustion, Nitrogen and Oxygen molecules in the induced air split into atomic species and combine to form NO. Along with NO, $NO_2$ is also partially formed. NO and $NO_2$ as a whole is known as $NO_x$.

$$\textit{Fuel Nitrogen} \rightarrow \textit{Nitrogen Intermediate} \rightarrow \mathrm{NO}\ \textit{or}\ \mathrm{N_2} \tag{14}$$

HC formation: HC is formed due to the exhaust of unburnt fuel. HC escapes from a combustion chamber due to quenched flame in the crevices and the reduced temperature of the chamber walls. It is also formed due to the cylinder-oil layer fuel absorption on the wall of the cylinder and that of the combustion chamber during cold starting. HC reduces with an increase in A/F ratio. The lean mixture is due to the poor quality of combustion, leading to engine misfiring and causing an erratic engine operation and a sharp increase in HC emission.

## 5. Finite Element Analysis of Coated Piston Design Exchange

FEA uses a technique to convert the entire piston to the number of discrete elements through meshing. It uses the auto-mesh provision of the ANSYS workbench to perform this function. The tetrahedral element type was chosen for the analysis, which has better error convergence and accuracy of the result output. In this analysis, conductive heat transfer through the coated piston surface is the dominant mode of thermal energy transfer. This is based on the assumption that there is no heat transfer effect on the engine piston system dynamics. There is no cavitation in ring-skirt and liner contact. Additionally, the effect of the ring twist is absent.

The mode of heat transfer in the oil is neglected. The thermal boundaries of the piston include the ring land, skirt, underside, and combustion side. The aligned boundary conditions state that the piston crown has direct exposure to hot gases or flame at a temperature of 400 °C. The maximum gas pressure in the combustion chamber is 12 MPa in an engine cycle. To avoid thermal expansion, wear, and rapid heat transfer, the piston material is considered of AlSi and cast steel materials; the details of material properties are listed in Table 2. Such materials are stronger against compressive stress and possess suitablethermal conductivity. Furthermore, bond-coated AlSi or steel make pistons enhance thermal distortion and wear resistance. Figure 2 represents the CAD model of type_A, B, C, and D pistons. As given in the figure, type_A has no bowl provision in the crown and crown type_B, C, and D pistons have different bowl shapes. In this study, the thickness of the NiCrAl bond coat was considered to be 100µm, which was kept constant, and

the thickness of the FGM was changed from 400µm to 1200µm at400µm increments, or the thickness of each inter-layer (70%$MgZrO_3$+30%NiCrAl, 50%$MgZrO_3$+ 50%NiCrAl, 30%$MgZrO_3$+70%NiCrAl) had been changed from 100µm to 400µm at100µm increment.

**Table 2.** Material properties of rigid elastic constituents.

| Materials | Thermal Conductivity (W/m °C) | Density (kg/m$^3$) | Specific Heat (J/kg °C) |
|---|---|---|---|
| Piston (AlSi) | 155 | 2700 | 960 |
| Piston (Steel) | 79 | 7870 | 500 |
| Bond coat (100%NiCrAl) | 16.1 | 7870 | 764 |
| 100%$MgZrO_3$ | 0.8 | 5600 | 650 |
| 70%$MgZrO_3$+30%NiCrAl | 4.6 | 6130.4 | 676.6 |
| 50%$MgZrO_3$+50%NiCrAl | 7.3 | 6543.7 | 697.39 |
| 30%$MgZrO_3$+70%NiCrAl | 10.4 | 7016.7 | 721.14 |
| Rings (cast iron) | 16 | 7200 | 460 |

The finite element model developed here is validated with a similar type of work by Buyukkya [26]. The piston profile is thus modified to validate geometry. The temperature distribution thus obtained is compared for AlSi and of uncoated thin-coated steel (0.4 mm) pistons. The result shows an adequate agreement with the fringe pattern of the temperature. The highest temperature value in the current case is slightly higher as compared to work reported by Buyukkya [26] for AlSi pistons. The solid model, mesh information, and output parameters of the analysis are listed in Supplementary Materials.

Table 2 shows the validation of crown center and bowl rim temperature from the FEA model by Buyukkya et al. [29]. In the majority of cases of comparison, the difference is less than 5%, except for both crown and bowl rim locations of the AlSi (UC). Table 3 shows the validation details of FEA model considering different piston materials.

**Table 3.** Details of FEA model validation.

| Sl. No. | Material | Temperature (°C) at Crown Centre [14] | Temperature (°C) at Crown Centre (Current) | Difference in Temperature | Temperature (°C) at Bowl Rim [14] | Temperature (°C) at Bowl Rim (Current) | Difference in Temperature |
|---|---|---|---|---|---|---|---|
| 1 | Steel (UC) | 333 | 357 | 7.20% | 357 | 372 | 4.20% |
| 2 | Steel (CT-0.4 mm) | 388 | 379 | −4.12% | 418 | 422 | 0.96% |
| 3 | AlSi (UC) | 285 | 325 | 14% | 270 | 315 | 16.67% |
| 4 | AlSi (CT-0.4 mm) | 342 | 358 | 4.6% | 366 | 380 | 3.82% |

## 6. Response Surface Methodology

The approach of response surface methodology (RSM) is generally used for the optimization of the process parameter and to find out the optimal conditions to improve the responses. Response surface methodology combines the test design parameters and output parameter optimization. RSM includes the input parameter design that gives a range of input variables in which the test is being conducted. By using a mathematical model, the relationship between the input and output variables are investigated and an optimal value of the input parameter is provided to build an ideal response [36]. Let us assume that all controlled variables ($a_1, a_2, \ldots, a_k$) and all the experiments are continuous, controllable, and measurable. The human error is ignored, so the linear output response r may be given as

$$r = f(a_1, a_2, \ldots\ldots, a_k) + \delta \quad (15)$$

where $\delta$ represents the different sources of the variable, which are not considered in $f$, or is also considered as the statistical error; the mean value of this statistical error is 0. The polynomials that are used in RSM is a second order, given as

$$r = \beta_0 + \sum_{i=1}^{k} \beta_i a_i + \sum_{i=1}^{k} \beta_{ii} a_i^2 + \sum_{i<j}\sum \beta_{ij} a_i r_j + \varepsilon \quad (16)$$

where the parameter $\beta_i$, $\beta_j$ = 0, 1, 2 . . . $k$ is the regression coefficient [37].

## 7. Results and Discussion

In our current investigation, we aimed to replace part of heavy gasoline with light methanol and to observe the carbon-redundant effects on fuel characteristics. Due to such exchange, fuel properties, such as calorific value, density, acid value, kinetic viscosity, flash point, auto-ignition temperature, and Octane number (RON and MON) must not deviate much from pure gasoline. Figure 3a–h show details of such fuel characteristic reformation due to carbon redundancy. For a 4.167% reduction in fuel carbon, replacement of $B_5$ (95% by volume of gasoline and 5% by volume of methanol) with gasoline yielded a 1.33% increase in calorific value, 0.077% increase in density, 6.6% increase in acid value, 1.15% increase in kinetic viscosity, 6% increase in flash point, 1.38% increase in auto-ignition temperature, and a 2.17% increase in Octane$^{RON}$ and 0.1% increase in Octane$^{MON}$.

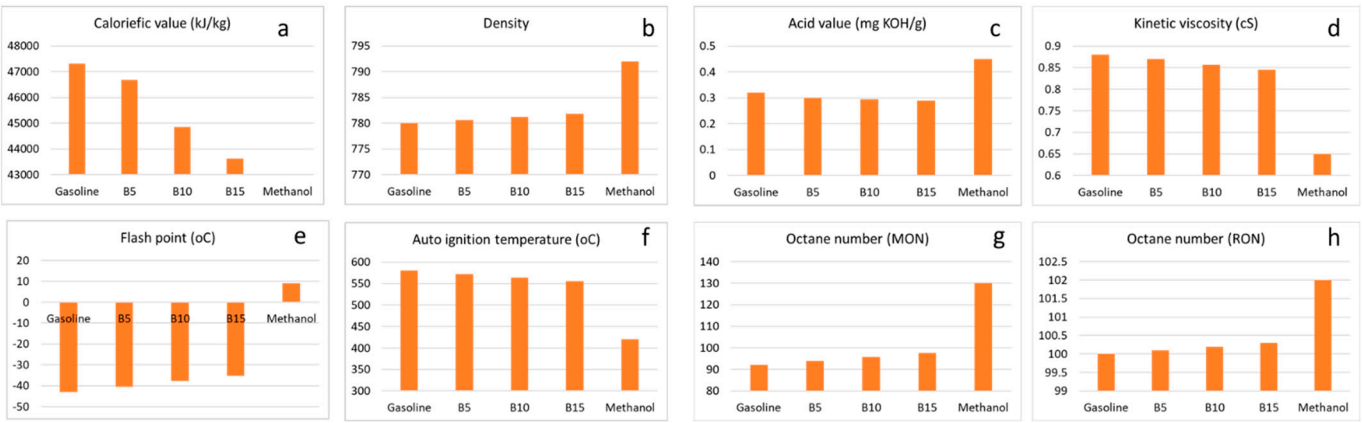


**Figure 3.** Fuel carbon redundancy effect on fuel characteristics: (**a**)calorific value(kJ/kg); (**b**)blend density (kg/m$^3$); (**c**) acid value (mg KOH/g); (**d**) fuel kinetic viscosity(cS); (**e**) flash point (°C); (**f**) autoignition temperature (°C); (**g**) octane number (MON); (**h**) octane number (RON).

Similarly, to achieve an 8.34% reduction in fuel carbon, $B_{10}$ (90% by vol. gasoline and 10% by vol. of methanol) is replaced with gasoline. This led to a 5.2% increase in calorific value, 0.15% increase in density, 7.8% increase in acid value, 2.6% increase in kinetic viscosity,1.2% increase in flash point, 2.76% increase in auto-ignition temperature, and a 4.13% increase in Octane$^{RON}$ and 0.2% increase in Octane$^{MON}$. Finally, to achieve a 12.5% reduction in fuel carbon, $B_{15}$ (85% by vol. gasoline and 15% by vol. of methanol) is replaced with gasoline. This led to a 0.154% increase in density, 3.79% increase in kinetic viscosity, 9.3% increase in acid value, 18% increase in flash point, 7.8% increase in calorific value, 4.1% increase in auto-ignition temperature, and a 6.2% increase in Octane$^{RON}$ and 0.3% increase in Octane$^{MON}$ observed. Changes in fuel characteristics due to fuel carbon redundancy is insignificant. In addition, corrosion effect and attack on the metal surface is negligible. Hence, these three different blends are expected to perform similarly to gasoline. Emission analysis can predict whether these are energy efficient or not. The numerical procedure as well as the experimental procedure (ASTM-based) are presented in the Methods subsection.

Figure 4a–d show the fuel carbon redundancy effect on emission formation at 1500 rpm for pistons with CT@0.8 mm and variable BMEP. For BMEP@2.38 bar, a 4% reduction in

fuel carbon ($B_5$) reduced the CO emission by 147.23 gm/kWh. Again, an 8%reduction in fuel carbon($B_{10}$), reduced the CO emission by 197.14 gm/kWh. Again, a 12% reduction in fuel carbon at BMEP@2.38 bar reduced the CO emission by 200.02 gm/kWh. For pure gasoline, as BMEP increased from 2.38 bar to 3.57 bar to 5.95 bar, the CO emission reduced from 232.34 gm/kWh to 109.16 gm/kWh to 162.67 gm/kWh, respectively. However, for all blends ($B_5$, $B_{10}$, and $B_{15}$), the CO emission increased with an increase in BMEP. The highest CO emission reduction was achieved at BMEP@2.38 bar for a 12% reduction in fuel carbon. The CO decreased with the increase in BMEP for gasoline, but increased for all the blended fuels. Figure 3b shows the variation of $CO_2$ due to fuel carbon reduction (−4%C, −8%C, and −12%C) through blend replacement by gasoline. In all cases (gasoline, $B_5$, $B_{10}$, and $B_{15}$), $CO_2$ emission decreased with an increase in BMEP (from 2.38 barto3.57 barto5.95 bar). It was observed that a 4% reduction in fuel carbon reduced $CO_2$ by 15.8 gm/kWh, 6.46 gm/kWh, and 17.96 gm/kWh for BMEP@2.38 bar,3.57 bar, and 5.95 bar, respectively. Furthermore, an 8% reduction in fuel carbon at these engine BMEP levels yielded $CO_2$ emissions at 0.8 gm/kWh, 7.18 gm/kWh, and 0.5 gm/kWh, respectively. Figure 3c shows the variation of $NO_x$ due to fuel carbon reduction (−4%C, −8%C, and −12%C). The maximum reduction of $NO_x$ occurred for B5(−4%C) (0.4114 gm/kWh) at BMEP@2.38 bar. Figure 3d shows the effect of lowering fuel carbon on the HC emission of the engine. With BMEP increased, the HC emission increased for gasoline and $B_5$. However, for $B_{10}$ and $B_{15}$, HC decreased. The lowest HC emission occurred at $B_{10}$(−8%C) for BMEP@3.57 bar and was found to be 0.02002 gm/kWh.

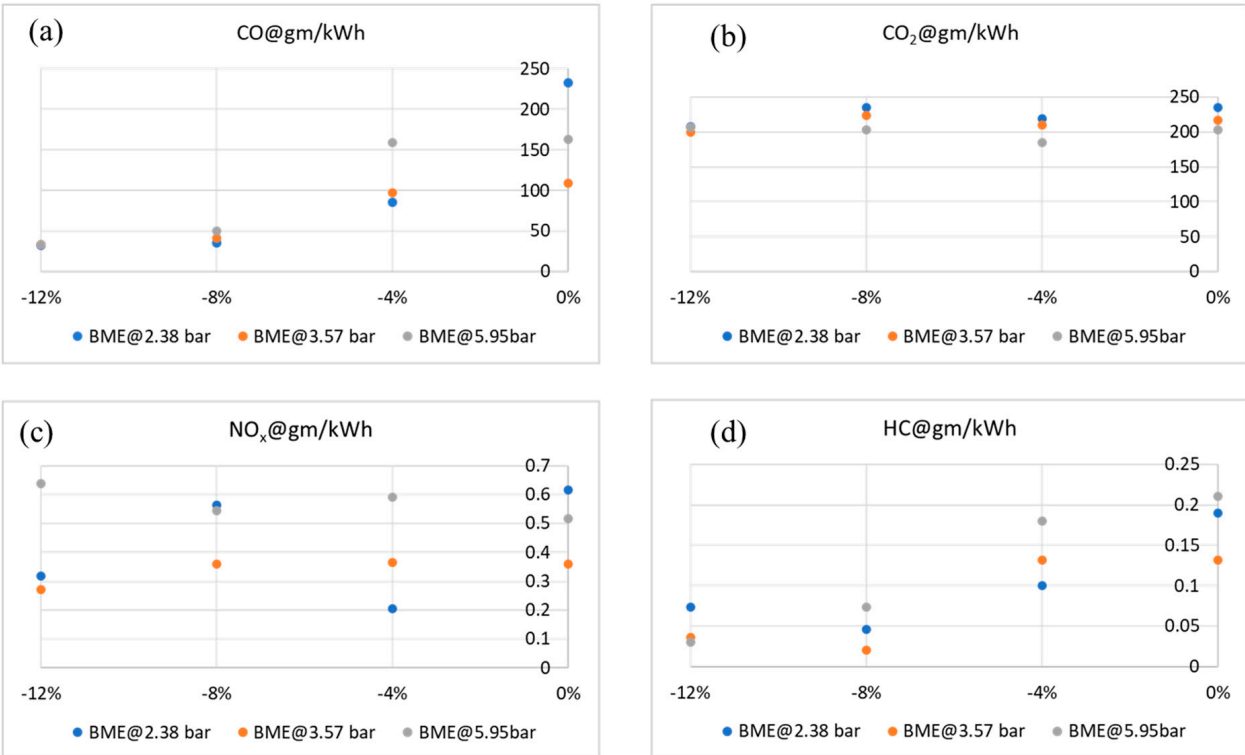


**Figure 4.** Fuel carbon redundancy effect on emission formation at 1500 rpm, CT@0.8 mm, and variable BMEP: (**a**) CO@gm/kWh; (**b**) $CO_2$@gm/kWh; (**c**) $NO_x$@gm/kWh; (**d**) HC@gm/kWh.

Figure 5a–d show CO, $CO_2$, $NO_x$, and HC emission variations due to fuel carbon removal through blending at 1500 rpm, BMEP@5.95 bar, and variable coating thicknesses. CO emission decreased with an increase in coating thickness. Fuel carbon removal of −4%C through blending ($B_5$) at the same condition lowered the CO emission (59.95 gm/kWh, 20.1 g/kWh, 3.95 gm/kWh, and 11.13 gm/kWh) for CT@uncoated at 0.4 mm, 0.8 mm, and 1.2 mm, respectively. Again, an 8% fuel carbon removal lowered the CO emission

by 176.77 gm/kWh, 177.29 g/kWh, 112.76 gm/kWh, and 105.13 gm/kWh, respectively. Similarly, a 12% fuel carbon removal ($B_{15}$) in the same condition lowered the CO emission by 215.45 gm/kWh, 133.22 g/kWh,129.64 gm/kWh, and 102.34 gm/kWh, respectively. In all cases except −12%C, the CO emission decreased with an increasing coating thickness, while in such an excepted case, the maximum emission occurred at CT@4 mm (64.2 gm/kWh). Figure 4b shows the carbon dioxide emission for different coating thicknesses. The $CO_2$ emission increased with an increase in coating thickness. Moreover, at a particular coating thickness, enhanced carbon removal elevates the $CO_2$ emission. In the uncoated piston condition, a 12% reduction in fuel carbon enhanced the $CO_2$ emission by 62.49 gm/kWh. Further to this analysis, for CT@0.4 mm,0.8 mm, and 1.2 mm, a maximum fuel carbon removal led to 34.48 g/kWh, 4.84 g/kWh, and 5.96 gm/kWh, respectively. The $CO_2$ emission was highest at −12 °C with aCT@1.2 mm and a value of 219.87 g/kWh. The details of the data related to all emissions are given in Supplementary Materials.

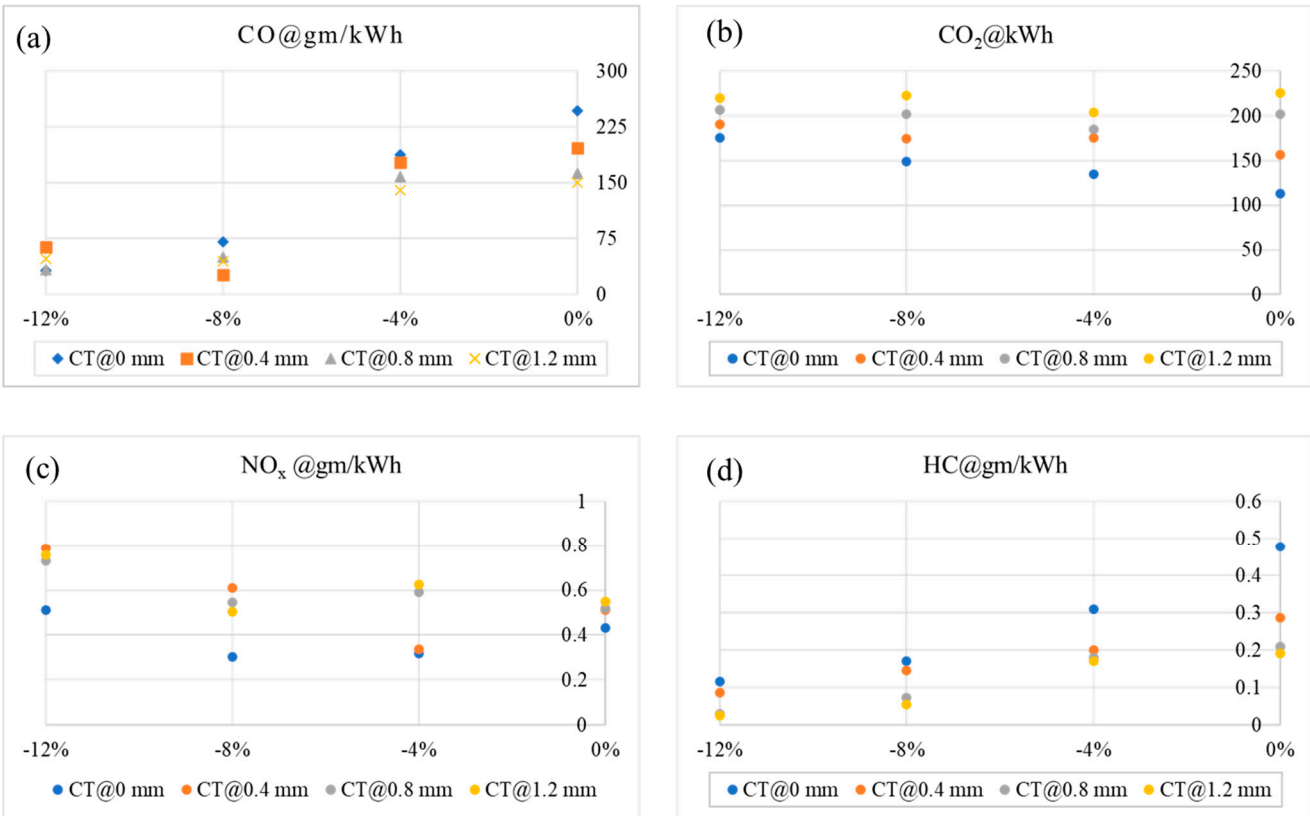


**Figure 5.** Fuel carbon redundancy effect on emission formation at 1500 rpm, BMEP@5.95 bar, and variable coating thicknesses: (**a**) CO@gm/kWh; (**b**) $CO_2$@gm/kWh; (**c**) $NO_x$@gm/kWh; (**d**) HC@gm/kWh.

Figure 5c shows the $NO_x$ emission for different coating thicknesses. $NO_x$ follows the same trend as $CO_2$. The maximum $NO_x$ level is 0.756 gm/kWh at B15 (−12%C) with a 1.2 mm coating thickness. The lowest $NO_x$ emission is 0.305 gm/kWh at (−8%C) for the uncoated condition. Figure 4d shows the HC emission for the same condition as described in Figure 5a–c. With an increase in carbon removal (−4%C,−8%C, and −12%C) for all coating thicknesses, HC decreases. Furthermore, in increasing, the HC emission decreases. A highest HC emission is 0.476 gm/kWh for pure gasoline in the uncoated condition, while the lowest is0.026 gm/kWh at (−12%C) with a 1.2 mm thickness.

Figure 6a–d show the fuel carbon redundancy effect on emission formation at 1500 rpm, 5.95 bar BMEP, CT@0.8 mm, and variable piston design exchange. Figure 6a shows that piston_D exhibiteda maximum CO emission (302 gm/kWh), while piston_C exhibited a mini-

mum CO emission (103.42 gm/kWh). Similarly, at −4%C, a maximum (242 gm/kWh, piston_C) and minimum (99.83 gm/kWh at piston_D)CO emission occurred. Again, for −8%C, a maximum (295.89 gm/kWh, piston_D) and minimum (48.47 gm/kWh, type_B)CO emission occurred. Finally, a 12% fuel carbon removal led to a maximum (280.45 gm/kWh, piston_D) and minimum (33 gm/kWh, piston_A)CO emission. For piston_A, CO emission decreased with carbon removal ($\Delta_{4\%}$@3.959 gm/kWh, $\Delta_{8\%}$@112.77 gm/kWh, and $\Delta_{12\%}$@129.67 gm/kWh). For the piston_B design ($\Delta_{4\%}$@98.13 gm/kWh, $\Delta_{8\%}$@149.49 gm/kWh, and $\Delta_{12\%}$@155.1 gm/kWh),a reduction in CO emission was observed. For the type_C design ($\Delta_{4\%}$@138.6 gm/kWh, $\Delta_{8\%}$@134.3 gm/kWh, and $\Delta_{12\%}$@155.85 gm/kWh),an increase in CO emission was observed. For the type_D piston design ($\Delta_{4\%}$@73.92 gm/kWh, $\Delta_{8\%}$@6.46 gm/kWh, and $\Delta_{12\%}$@21.91 gm/kWh),a reduction in CO emission wasobserved.

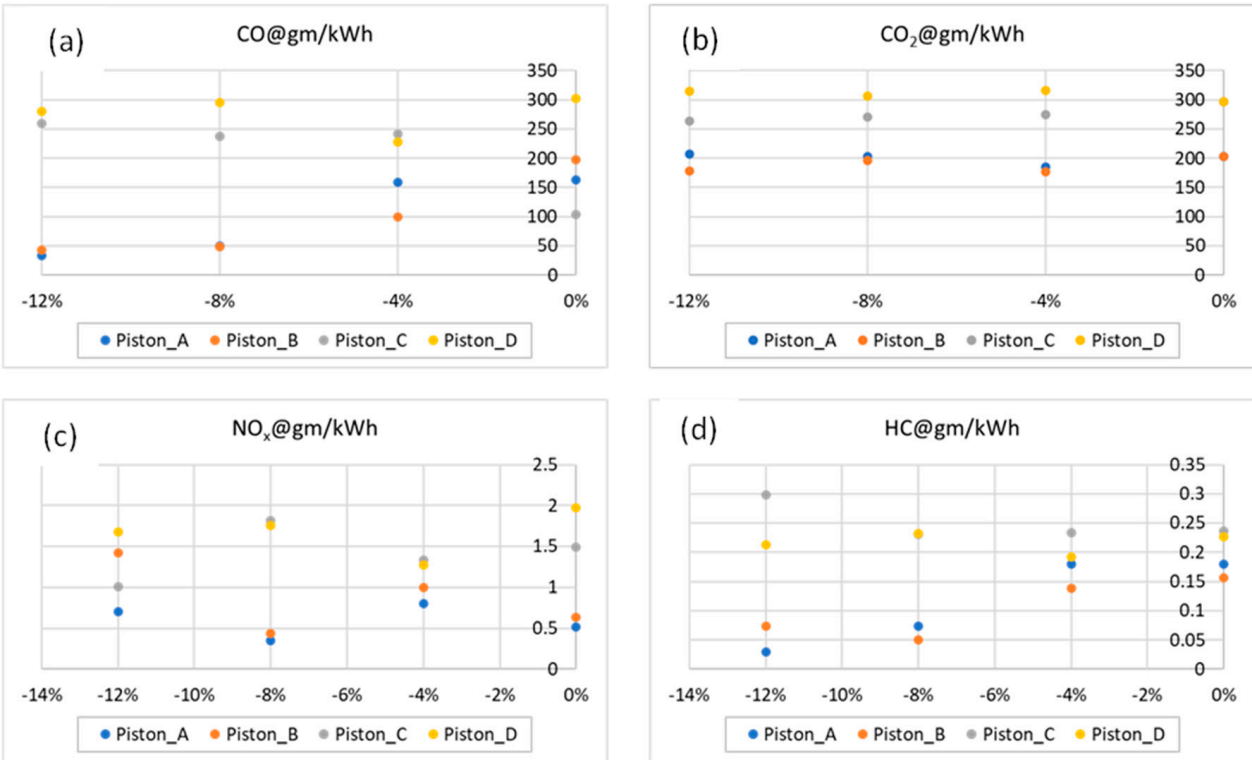


**Figure 6.** Fuel carbon redundancy effect on emission formation at 1500 rpm, BMEP@5.95 bar, CT@0.8 mm, and variable piston design exchange: (**a**) CO@gm/kWh; (**b**) $CO_2$@gm/kWh; (**c**) $NO_x$@gm/kWh; (**d**) HC@gm/kWh.

Figure 6b shows the effect of fuel carbon reduction on $CO_2$ emission considered for different piston design exchange. Maximum $CO_2$ emission occurred at −4%C for type_D piston and was found to be 316.7 gm/kWh, and the lowest was 177.4 gm/kWh for piston_B. A higher carbon removal reduced the $CO_2$ emission in the type_C piston design while, in case of type_D, it increased. There is a mixed trend in the case of piston_A and piston_B. For type_A piston, the $CO_2$ ($\Delta_{4\%}$@17.93 gm/kWh, $\Delta_{8\%}$@0.6 gm/kWh, and $\Delta_{12\%}$@-4.34 gm/kWh) decreased with the corresponding fuel carbon reduction. Similar was the case for the $CO_2$ emission of piston_B($\Delta_{4\%}$@25.13 gm/kWh, $\Delta_{8\%}$@5.75 gm/kWh, and $\Delta_{12\%}$@23.79 gm/kWh). For piston design exchange type_C, $CO_2$ emission ($\Delta_{4\%}$@21.61 gm/kWh, $\Delta_{8\%}$@25.61 gm/kWh, and $\Delta_{12\%}$@32.31 gm/kWh) reduced. Finally, for piston_D ($\Delta_{4\%}$@-19.38 gm/kWh, $\Delta_{8\%}$@-8.61 gm/kWh, and $\Delta_{12\%}$@-17.95 gm/kWh) reduction was achieved.

Figure 6c shows the $NO_x$ emission variation due to piston design exchange at 1500 rpm, BMEP@5.95 bar, and CT@0.8 mm. The maximum $NO_x$ emission occurred at piston_D using gasoline (1.97 gm/kWh). The lowest emission occurred in the case of piston design_A (0.35 gm/kWh), In the type_A piston, $NO_x$ formation changes ($\Delta_{4\%}$@-0.285 gm/kWh,

$\Delta_{8\%}$@0.165 gm/kWh, and $\Delta_{12\%}$@-0.186 gm/kWh) were observed. For design_B, $NO_x$varies ($\Delta_{4\%}$@-0.372 gm/kWh, $\Delta_{8\%}$@-0.2 gm/kWh, and $\Delta_{12\%}$@-0.79 gm/kWh). Again, for piston_C, $\Delta_{4\%}$@0.15 gm/kWh, $\Delta_{8\%}$@-0.34 gm/kWh, and $\Delta_{12\%}$@-0.48 gm/kWh was observed. Finally, for piston_D, $\Delta_{4\%}$@0.16 gm/kWh, $\Delta_{8\%}$@0.21 gm/kWh, and $\Delta_{12\%}$@0.3 gm/kWh was observed. Figure 6d shows the HC variation due to piston design exchange. The minimum HC emission is 0.03 gm/kWh due to a 12% reduction in fuel carbon and design_A implementation. The maximum HC emission observed in this study is 0.29 gm/kWh in the case of design exchange_C due to a 12% fuel carbon reduction. In case of piston_A ($\Delta_{4\%}$@0.05 gm/kWh, $\Delta_{8\%}$@0.106 gm/kWh, and $\Delta_{12\%}$@0.15 gm/kWh), a reduction in HC emission was observed compared to gasoline. Similarly, for design exchange B, C, and D, $\Delta_{4\%}$@0.018 gm/kWh, $\Delta_{8\%}$@0.51 gm/kWh, and $\Delta_{12\%}$@0.082 gm/kWh; $\Delta_{4\%}$@0.002 gm/kWh, $\Delta_{8\%}$@0.006 gm/kWh, and $\Delta_{12\%}$@-0.062 gm/kWh; and $\Delta_{4\%}$@0.034 gm/kWh, $\Delta_{8\%}$@-0.06 gm/kWh, and $\Delta_{12\%}$@0.014 gm/kWh was observed, respectively.

The energy and efficiency of an engine is greatly influenced by the exhaust performance parameters, such as temperature, back pressure, exhaust gas density, muffler noise, etc. In the context of piston design exchange and fuel carbon reduction through blending, Figure 7a–d show the effect on such parameters. Figure 7a shows the temperature variation. The maximum temperature variation is 360 °C when using gasoline. Replacing gasoline with $B_5$(−4%C) reduced the exhaust temperature by 5.5 °C. Similarly, replacing gasoline with $B_{10}$(−8%C) and $B_{15}$(−12% C) reduced the exhaust temperature by 3 °C and 3.5 °C, respectively. An increase in the exhaust temperature beyond some limit is not energy-efficient, or engine-friendly. Figure 7b shows the effect of a low-carbon fuel option on back pressure. Piston C and D designs developed more back pressure compared to the A and B designs. Replacing gasoline with $B_5$, $B_{10}$, and$B_{15}$, the back pressure increased by $\Delta_{4\%}$@0.0095 MPa, $\Delta_{8\%}$@0.02 MPa, and $\Delta_{12\%}$@0.0344 MPa for design A. Similarly, the back pressure increment was observed to be $\Delta_{4\%}$@0.0095 MPa, $\Delta_{8\%}$@0.0233 MPa, and $\Delta_{12\%}$@0.032 MPa; $\Delta_{4\%}$@0.088 MPa, $\Delta_{8\%}$@0.02 MPa, and $\Delta_{12\%}$@0.0109 MPa; and $\Delta_{4\%}$@0.0199 MPa, $\Delta_{8\%}$@0.002 MPa, and $\Delta_{12\%}$@0.029 MPa for B, C, and D, respectively. Figure 7c shows the density variation of exhaust gas. The gas density indirectly affects the energy efficiency as it interlinks combustion and operation. The maximum gas density of 1.228 kg/m$^3$ was observed for piston_D at a 12% fuel carbon reduction. The lowest density variation was1.221 kg/m$^3$ for piston_A when using pure gasoline. Figure 7d shows the bar chart of the noise level at exhaust measured in dB. In all other cases except type_C, the maximum noise level is at −4%C fuel carbon removal. Piston_Dhas a higher noise level compared to other designs. In almost all cases, an increase in the % of carbon removal reduces the noise level. The combined effect of design exchange and fuel carbon removal can reduce noise level up to 2.32% for piston_A,3.18% for piston_B, 2.46% for piston_C, and 1.1% for piston_D.

The operational efficiency of the engine system depends on the thermal conductivity of the piston material. For better energy efficiency, the temperature retention of a metallic piston plays an important role. The life expectancy, frictional behavior, and decarbonization potential are largely affected by this tendency. The selected suitable material and coating can be altered. The gas pressure is one of the load considerations for piston design exchange. For a high strength-to-weight ratio and better heat rejection, two different piston materials (AlSi and Steel) are considered here along with NiCrAl as a bond coat: 70% $MgZrO_3$ + 30% NiCrAl as a main coating. Detailed properties of the piston, bond coat, and coating material are given in an above table, which includes thermal conductivity, density, and specific heat. Finite element analysis is carried out, the details of which is given in the methods section. Figure 8a–h show the FEA simulated temperature for steel and AlSi pistons for four different designs (A, B, C, D). For the steel piston, the maximum temperature increases with an increase in coating thickness. The highest temperature of 391 °C developed for the uncoated type_A piston. For the coated piston, 422 °C@type_BwithCT@0.4 mm, 582 °C@type_CwithCT@0.8 mm, and 598 °C@type_DwithCT@1.2 mm was observed. For the AlSi piston, the maximum temperature rise occurred at 340 °C for the uncoated type_B, at 392 °C with a CT@0.4 mm for type_B, at 516 °C fortype_C with a CT@0.8 mm, and

593 °C with a CT@1.2 mm for piston_A, for the same coating thickness and piston type. AlSi developed a lower temperature compared to steel because of more conductivity in the former case. A maximum temperature reduction of 13% is possible by replacing AlSi with steel.

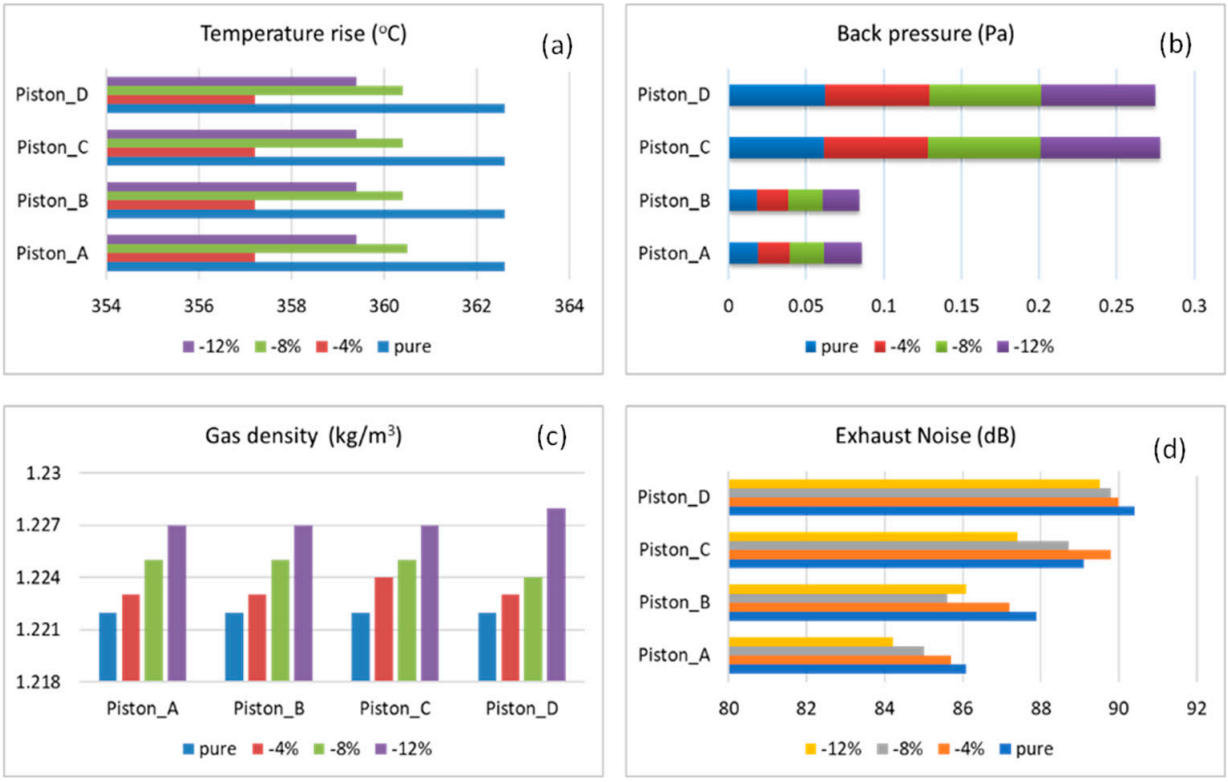


**Figure 7.** Bar chart of fuel carbon redundancy effect on energy influencing parameters: (**a**) temperature rise, (**b**)back pressure variations, (**c**)density variation, and (**d**) exhaust noise.

Figure 9a–f show the strain energy and interlinked parameters (von-Mises stress and elastic deformation) in response to piston design exchange and variable coating thicknesses. As part of the total energy, strain energy plays a considerable role in energy efficiency. The lower the strain energy due to resilience, the higher the back power available to the wheel. Figure 9a,b show the resilience for pistons of different designs (A, B, C, D) with variable coating thicknesses. For the AlSi piston, a better strain energy for the type_B piston with CT@0.8 mm occurs (240 kJ/kg). With the increase in CT for all designs, strain energy increases up to CT@0.8 mm and then decreases. For both AlSi and steel, in all cases of coating, the order of strain energy is type_B > type_C > type_D >type_A. Figure 8c,d show the von-Mises response to the above stated conditions. The highest is 1332 MPa for the type_BAlSi piston with CT@0.4 mm. Figure 8e,f show the elastic deformation in the stated load and boundary conditions. For all the contemporary cases, the AlSi piston shows more deformation than the steel piston.


**Figure 8.** Effect of piston design exchange and coating thickness on energy influencing parameter (temperature, in °C)., (**a**) Steel with CT= 0 mm; (**b**) Steel with CT =0.4 mm; (**c**) AlSi with CT = 0 mm; (**d**) AlSi with CT=0.4 mm; (**e**) Steel with CT =0.8 mm; (**f**) Steel with CT= 1.2 mm; (**g**) AlSi with CT =0.8 mm; (**h**) AlSi with CT = 1.2 mm.


**Figure 9.** (**a**–**f**) Strain energy and interlinked parameters (von-Mises stress and elastic strain) response to piston design exchange and variable coating thicknesses.

## 8. Evolution of Mathematical Model—Design of Experiment for Response Surface Methodology

Here, we demonstrate the effect of $A_1(\delta)$, $B_1$(CT), and $C_1$(E) and $A_2$(Blend), $B_2$(BMEP), and $C_2$(N) at six independent variables with three levels. The variables shown in Table 4 were independent variables selected for optimization.

**Table 4.** Independent variables used for Box–Behnken design for optimization.

| Variables | Symbol | Unit | Level | | |
|---|---|---|---|---|---|
| | | | −1 | 0 | 1 |
| δ | $A_1$ | mm | 2 | 3.5 | 5 |
| CT | $B_1$ | mm | 0 | 0.4 | 0.8 |
| E | $C_1$ | GPa | 200 | 215 | 230 |
| Blend | $A_2$ | % | 5 | 3.5 | 15 |
| BMEP | $B_2$ | bar | 2.98 | 3.57 | 5.95 |
| N | $C_2$ | rpm | 500 | 1000 | 1500 |

Independent variables used for the Box–Behnken design to optimize the effect of $A_1(\delta)$, $B_1$(CT), and $C_1$(E) and $A_2$(Blend), $B_2$(BMEP), and $C_2$(N) at three levels is shown in Tables 4 and 5. A total of 17 datapoints were taken separately to get the response for $D_{elastic}$, $\sigma_{von\text{-}Mises}$, and $T_{surface}$, and CO, $CO_2$, $NO_x$, and HC. The variables shown in Tables 5 and 6 were independent variables selected for optimization.

**Table 5.** Details of actual vs. predicted responses of output parameters (elastic).

| Run | δ | CT | E | $D_{elastic}$ | | $\sigma_{von\text{-}Mises}$ | | $T_{surface}$ | |
|---|---|---|---|---|---|---|---|---|---|
| | | | | Actual | Predicted | Actual | Predicted | Actual | Predicted |
| 1 | 5 | 0.8 | 215 | 0.3935 | 0.3891 | 306 | 158.38 | 379 | 404.63 |
| 2 | 3.5 | 0.4 | 215 | 0.3855 | 0.3855 | 317.7 | 317.7 | 341 | 341 |
| 3 | 2 | 0.4 | 230 | 0.3872 | 0.3812 | 872 | 755.75 | 375 | 361.75 |
| 4 | 5 | 0.4 | 200 | 0.211 | 0.217 | 247 | 363.25 | 379 | 392.25 |
| 5 | 5 | 0.4 | 230 | 0.4345 | 0.424 | 232 | 309.5 | 324 | 323.5 |
| 6 | 2 | 0.8 | 215 | 0.3615 | 0.3526 | 678 | 724.13 | 415 | 453.38 |
| 7 | 3.5 | 0.8 | 200 | 0.1964 | 0.1948 | 470 | 501.38 | 582 | 543.13 |
| 8 | 3.5 | 0 | 230 | 0.3874 | 0.389 | 234 | 202.62 | 315 | 353.88 |
| 9 | 3.5 | 0.4 | 215 | 0.3855 | 0.3855 | 317.7 | 317.7 | 341 | 341 |
| 10 | 5 | 0 | 215 | 0.3738 | 0.3827 | 79 | 32.88 | 333 | 294.63 |
| 11 | 2 | 0 | 215 | 0.3684 | 0.3728 | 95 | 242.62 | 340 | 314.38 |
| 12 | 3.5 | 0.4 | 215 | 0.3855 | 0.3855 | 317.7 | 317.7 | 341 | 341 |
| 13 | 3.5 | 0.4 | 215 | 0.3855 | 0.3855 | 317.7 | 317.7 | 341 | 341 |
| 14 | 3.5 | 0 | 200 | 0.2278 | 0.2129 | 133 | 62.87 | 379 | 404.13 |
| 15 | 2 | 0.4 | 200 | 0.2031 | 0.2136 | 770 | 692.5 | 422 | 422.5 |
| 16 | 3.5 | 0.4 | 215 | 0.3855 | 0.3855 | 317.7 | 317.7 | 341 | 341 |
| 17 | 3.5 | 0.8 | 230 | 0.3785 | 0.3934 | 301 | 371.13 | 489 | 463.88 |

**Table 6.** Details of actual vs. predicted responses of output parameters (emission).

| Run | Blend | BMEP | N | CO | | $CO_2$ | | $NO_x$ | | HC | |
|---|---|---|---|---|---|---|---|---|---|---|---|
| | | | | Actual | Predicted | Actual | Predicted | Actual | Predicted | Actual | Predicted |
| 1 | 10 | 2.38 | 500 | 59.8401 | 67.97 | 264.035 | 256.31 | 264.035 | 0.1196 | 0.584848 | 0.4668 |
| 2 | 5 | 3.57 | 500 | 311.061 | 272.37 | 247.533 | 260.61 | 247.533 | 0.2748 | 1.05007 | 0.4668 |
| 3 | 5 | 2.38 | 1000 | 149.87 | 193.32 | 257.688 | 247.97 | 257.688 | 0.3231 | 0.618078 | 0.4668 |
| 4 | 10 | 3.57 | 1000 | 53.91 | 53.91 | 302.117 | 302.12 | 302.117 | 0.2856 | 0.212672 | 0.4668 |
| 5 | 10 | 3.57 | 1000 | 53.91 | 53.91 | 302.117 | 302.12 | 302.117 | 0.2856 | 0.212672 | 0.4668 |
| 6 | 5 | 5.95 | 1000 | 210.788 | 204.62 | 265.305 | 282.94 | 265.305 | 0.4997 | 1.09659 | 0.4668 |
| 7 | 15 | 5.95 | 1000 | 231.274 | 200.25 | 272.286 | 284.64 | 272.286 | 0.3069 | 0.578202 | 0.4668 |
| 8 | 15 | 3.57 | 500 | 53.3709 | 51.97 | 299.578 | 320.57 | 299.578 | 0.0821 | 0.219318 | 0.4668 |
| 9 | 10 | 5.95 | 1500 | 55.5273 | 60.76 | 341.469 | 337.83 | 341.469 | 0.5105 | 0.16615 | 0.4668 |
| 10 | 10 | 2.38 | 1500 | 15.6339 | −29.69 | 265.305 | 303.01 | 265.305 | 0.3339 | 1.47541 | 0.4668 |
| 11 | 15 | 3.57 | 1500 | 44.7453 | 83.43 | 338.93 | 325.85 | 338.93 | 0.2964 | 0.186088 | 0.4668 |
| 12 | 10 | 5.95 | 500 | 107.82 | 139.78 | 300.848 | 274.5 | 300.848 | 0.2961 | 0.252548 | 0.4668 |
| 13 | 5 | 3.57 | 1500 | 56.6055 | 58.01 | 380.82 | 359.82 | 380.82 | 0.4891 | 0.259194 | 0.4668 |
| 14 | 15 | 2.38 | 1000 | 55.5273 | 49.27 | 286.884 | 266.61 | 286.884 | 0.1304 | 0.385468 | 0.4668 |
| 15 | 10 | 3.57 | 1000 | 53.91 | 53.91 | 302.117 | 302.12 | 302.117 | 0.2856 | 0.212672 | 0.4668 |
| 16 | 10 | 3.57 | 1000 | 53.91 | 53.91 | 302.117 | 302.12 | 302.117 | 0.2856 | 0.212672 | 0.4668 |
| 17 | 10 | 3.57 | 1000 | 53.91 | 53.91 | 302.117 | 302.12 | 302.117 | 0.2856 | 0.212672 | 0.4668 |

For the determination of the predicted value of all responses, the coded and actual regression equations are shown. For regression equation, design software v8.0 was used.

For $D_{elastic}$:

In terms of the coded factor:

$$\text{Coded Equation} = 0.3855 + 0.011575\,A - 0.0034375\,B + 0.0936625\,C + 0.00665\,AB + 0.00985\,AC + 0.005625\,BC + 0.0001125\,A^2 - 0.0113125\,B^2 - 0.0766625\,C^2 \quad (17)$$

In terms of the actual factor:

$$\text{Actual Equation} = -16.3156 - 0.0911889\ A - 0.192385\ B + 0.150848\ C + 0.0110833\ AB + 0.000437778\ AC + 0.0009375\ BC + 0.00005\ A^2 - 0.0707031\ B^2 - 0.000340722\ C^2 \quad (18)$$

For $\sigma_{\text{von-Mises}}$:
In terms of the coded factor:

$$\text{Coded equation} = 317.7 - 193.875\ A + 151.75\ B + 2.375\ C - 89\ AB - 29.25\ AC - 67.5\ BC + 108.775\ A^2 - 136.975\ B^2 + 103.775\ C^2 \quad (19)$$

In terms of the actual factor:

$$\text{Actual Equation} = 20{,}206.1 - 128.828 * A + 4002.17\ B - 189.117\ C - 148.333\ AB - 1.3\ AC - 11.25\ BC + 48.3444\ A^2 - 856.094\ B^2 + 0.461222\ C^2 \quad (20)$$

For $T_{\text{surface}}$:
In terms of the coded factor:

$$\text{Coded Equation} = 341 - 17.125\ A + 62.25\ B - 32.375\ C - 7.25\ AB - 2\ AC - 7.25\ BC - 20.25\ A^2 + 46 * B^2 + 54.25\ C^2 \quad (21)$$

In terms of the actual factor:

$$\text{Actual Equation} = 11{,}676.1 + 75.5278\ A + 227.708\ B - 105.042\ C - 12.0833\ AB - 0.0888889\ AC - 1.20833 * BC - 9\ A^2 + 287.5\ B^2 + 0.241111\ C^2 \quad (22)$$

For CO:
In terms of the coded factor:

$$\text{Coded equation} = 65.9218 + -37.1057 * A + 40.5673 * B + -44.1707 * C + 34.9209 * AB + 61.4574 * AC + 4.66038 * BC + 82.3475 * A^2 + 13.5954 * B^2 + -19.8119 * C^2 \quad (23)$$

In terms of the actual factor:

$$\text{Actual Equation} = 888.522 + -114.179 * A + -57.1656 * B + -0.197424 * C + 3.91271 * AB + 0.024583 * AC + 0.00522171 * BC + 3.2939 * A^2 + 4.26694 * B^2 + -7.92477 \times 10^{-5} * C^2 \quad (24)$$

For $CO_2$:

$$\text{Coded equation} = 310.547 + 5.08595 * A + 13.2494 * B + 27.5092 * C + -4.23412 * AB + -23.4839 * AC + 4.15896 * BC + 3.88754 * A^2 + -36.1184 * B^2 + 18.4856 * C^2 \quad (25)$$

$$\text{Actual Equation} = -18.0973 + 15.4967 * A + 101.934 * B + -0.0183395 * C + -0.474411 * AB + -0.00939356 * AC + 0.00465989 * BC + -0.155502 * A^2 + -11.3358 * B^2 + 7.39426 \times 10^{-5} * C^2 \quad (26)$$

For $NO_x$:

$$\text{Coded Equation} = 0.315039 + -0.096367 * A + 0.0882749 * B + 0.107167 * C \quad (27)$$

$$\text{Actual Equation} = 0.0874646 + -0.0192734 * A + 0.0494537 * B + 0.000214333 * C \quad (28)$$

For HC:

$$\text{Coded equation} = 0.466784 \quad (29)$$

$$\text{Actual Equation} = 0.466784 \quad (30)$$

The plot between the predicted and actual value of all the responses is shown in Figure 10a,b.The predicted value is reasonably near to the experimental value so the correlation between the predicted and experimental value is validated.

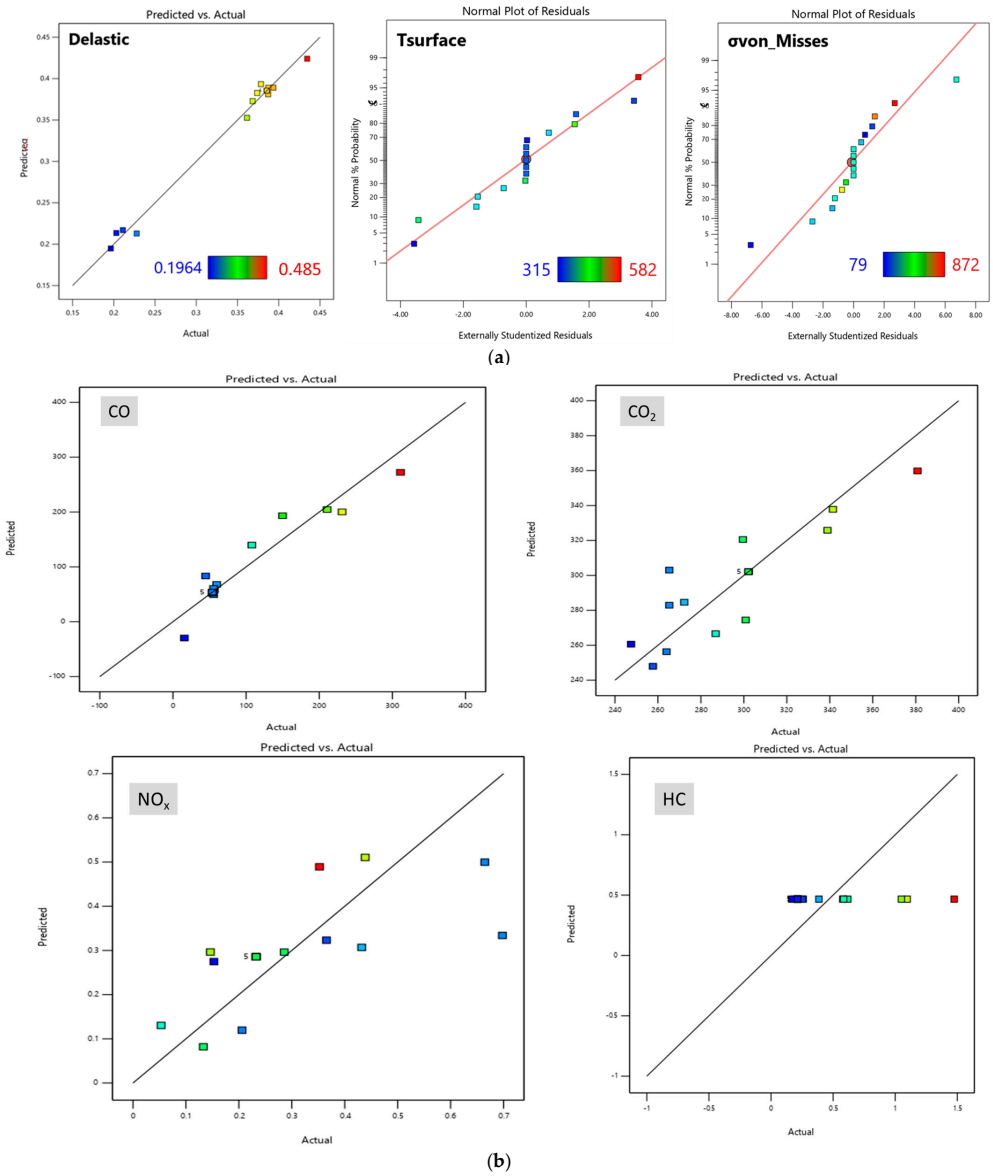


**Figure 10.** Predicted vs. actual value of output parameters: (**a**) elastic response, (**b**) emission response.

The effects of the input process variable on the different output parameter can be seen. It can be observed that E has substantial effects on all output parameters among all reaction parameters. Figure 11a,b show the Box–Cox plot of elastic response and emission response, respectively. It transforms the elastic and emission data to close to normal distribution. Figure 12a–b show the perturbation plot for the output variable, which is from a mathematical method, to find the approximate values of elastic and emission parameters. Here it is observed that there is a single point on the perturbation plot of HC emission due to zero influence on currently considered input parameters.

Figures 13–15 show the 3D plot for comparative analysis of the maximum value of elastic deformation, von Mises, and surface temperature in response to CT-delta, E-delta, and E-CT, respectively. Similarly, Figures 16–18 show the same 3D plot for emission constituents like CO, $CO_2$, $NO_x$, and HC, respectively.

### 8.1. Effect on Reaction Parameter

The three-dimensional curves were drawn to investigate the effect of the independent process parameter on the dependent process parameter. These graphs were drawn by taking two other parameters at the zero level.

### 8.2. Effect on $D_{elastic}$

It can be seen in the 3D counter plot in Figure 13a that when E is held constant, the variation of $D_{elastic}$ is constant with respect to the other two parameters. Figure 13b shows that when CT is held constant, $D_{elastic}$ decreases with respect to E and δ. Figure 13c shows that when δ is held constant, $D_{elastic}$ decreases with respect to E and CT.

### 8.3. Effect on Surface Temperature

Figure 15 shows the effect of various input parameters on surface temperature. It can be observed in Figure 15a that when E is held constant, the surface temperature rapidly decreases and then gradually increases with respect to CT and δ. Figure 15b shows that when CT is held constant, the surface temperature gradually decreases and then rapidly increases with respect to the other two parameters E and δ. Figure 15c shows that when δ is held constant, the surface temperature increases with respect to E and CT.

### 8.4. Optimization of Parameter

The optimization of individual input parameters was performed to achieve the minimum of $D_{elastic}$, maximum of von Mises stress, and minimum surface temperature. The optimal value of all input parameters is given in Table 7. The predicted value of all input variables, providing positive agreement with the simulation result, is shown in Table 8.

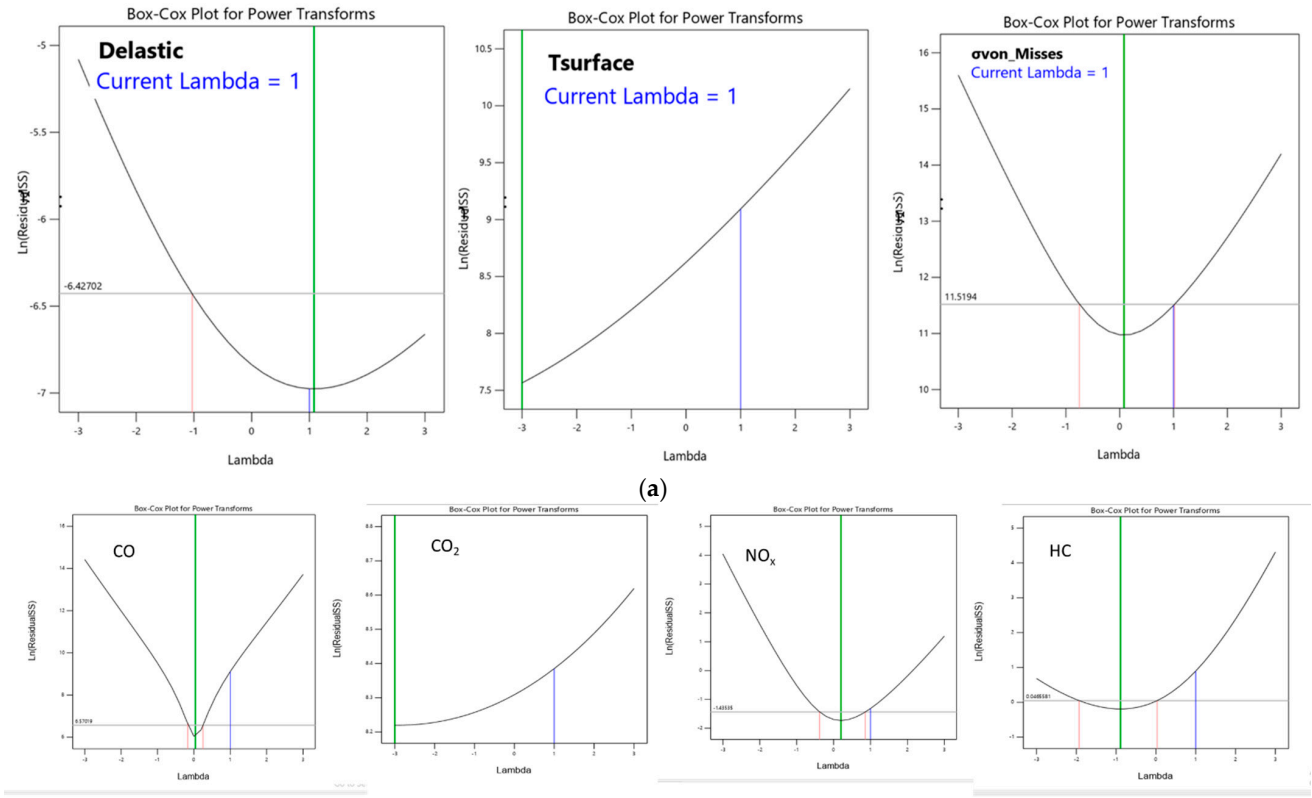


**Figure 11.** Box–Cox plot for power transform:(**a**) elastic response, (**b**)emission response.

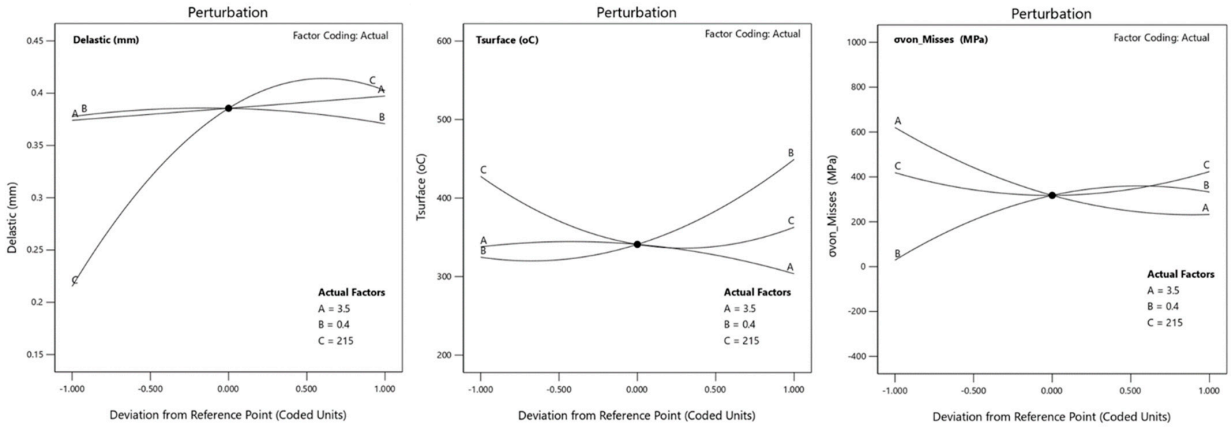


(**a**)

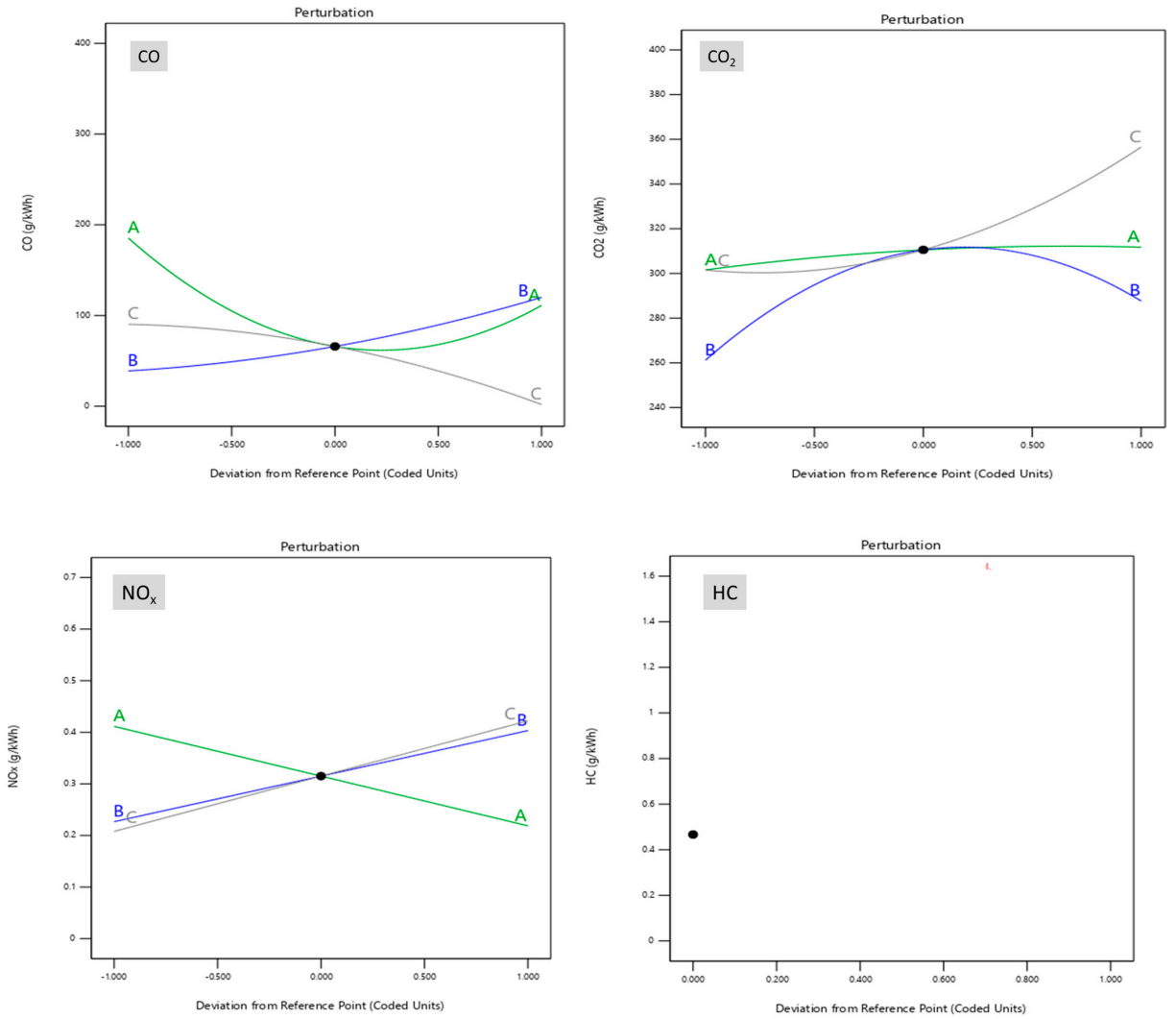


(**b**)

**Figure 12.** Perturbation for the output variables: (**a**) elastic response, (**b**)emission response.

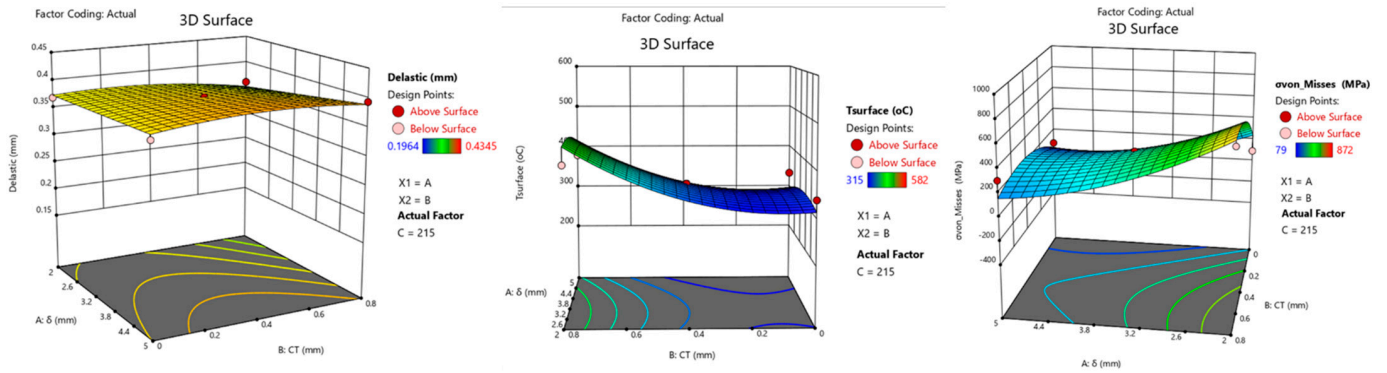


**Figure 13.** Comparative analysis of maximum elastic deformation (response to CT-delta; E-Delta and E-CT).

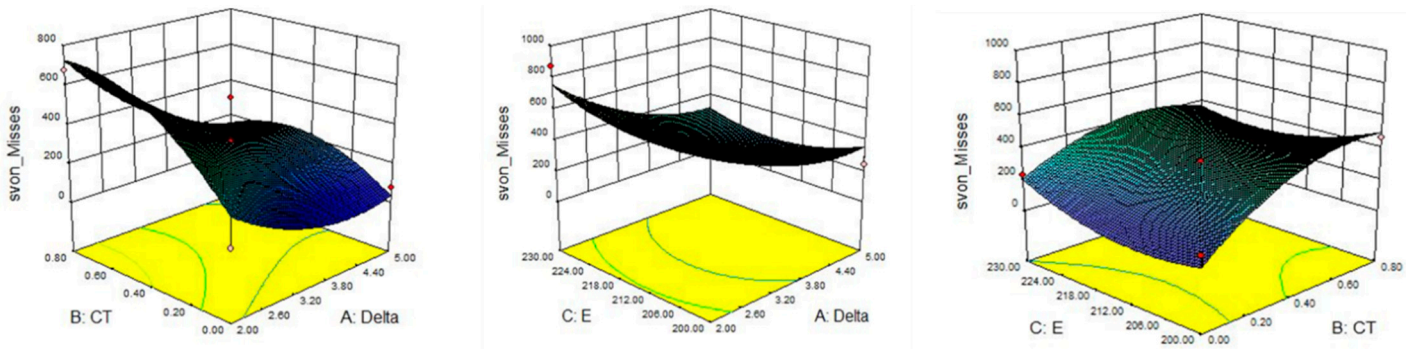


**Figure 14.** Comparative analysis of maximum von-Mises stress (response to CT-delta; E-Delta and E-CT).

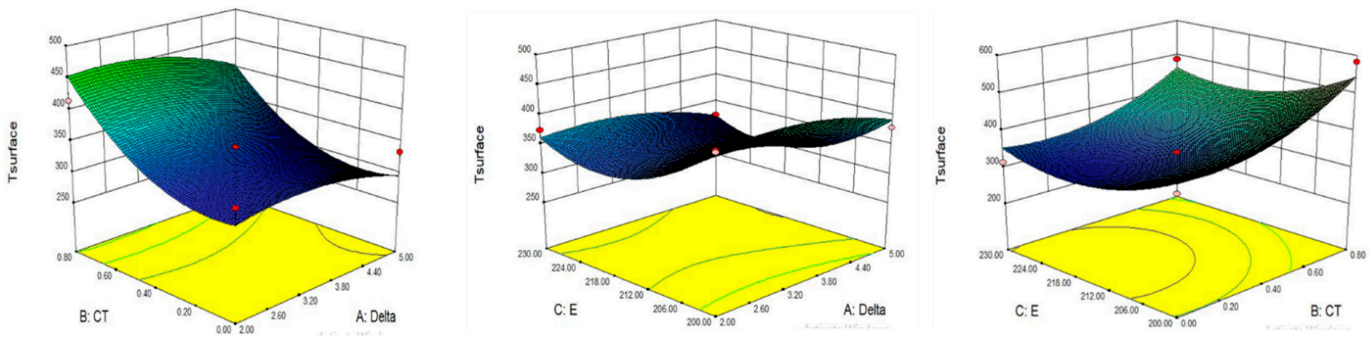


**Figure 15.** Comparative analysis of maximum surface temperature (response to CT-delta; E-Delta; E-CT).

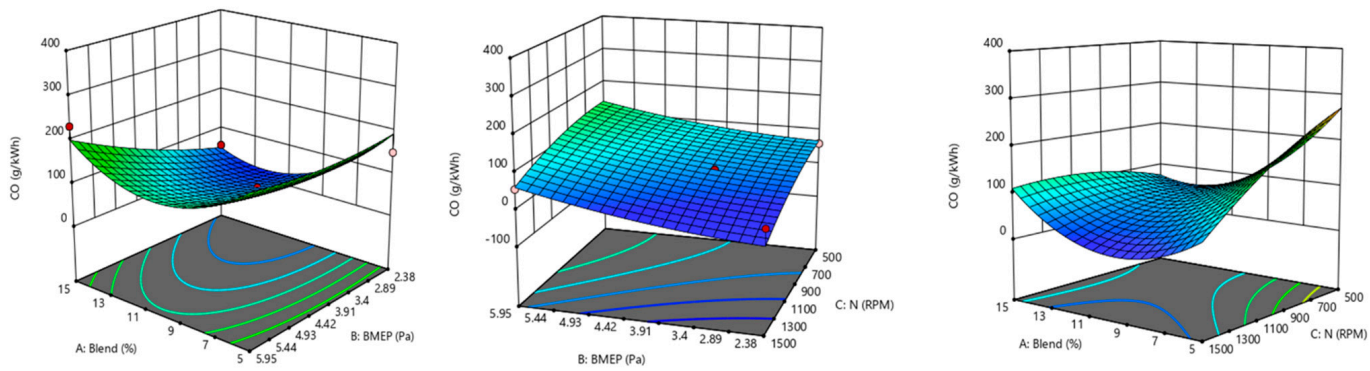


**Figure 16.** Comparative analysis of maximum CO emission (response to blend-BMEP; BMEP-N; Blend-N).

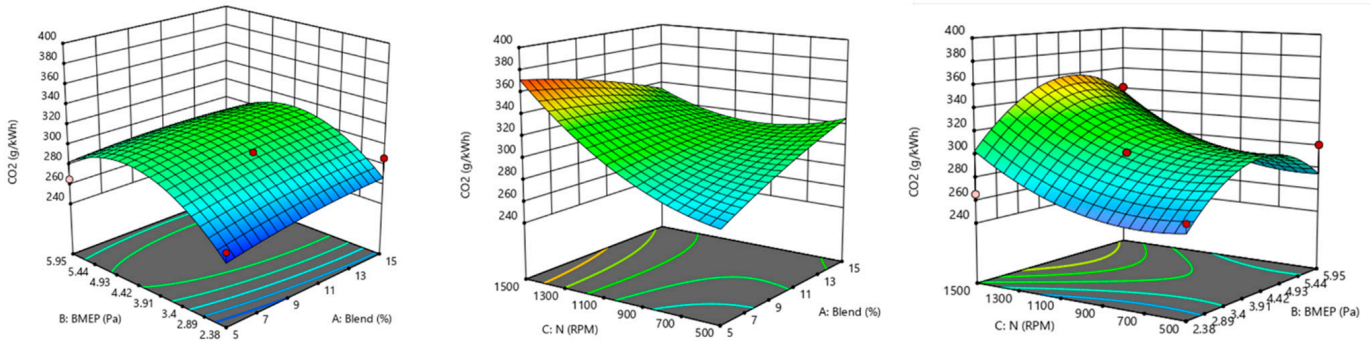


**Figure 17.** Comparative analysis of maximum $CO_2$ emission (response to blend-BMEP; BMEP-N; Blend-N).

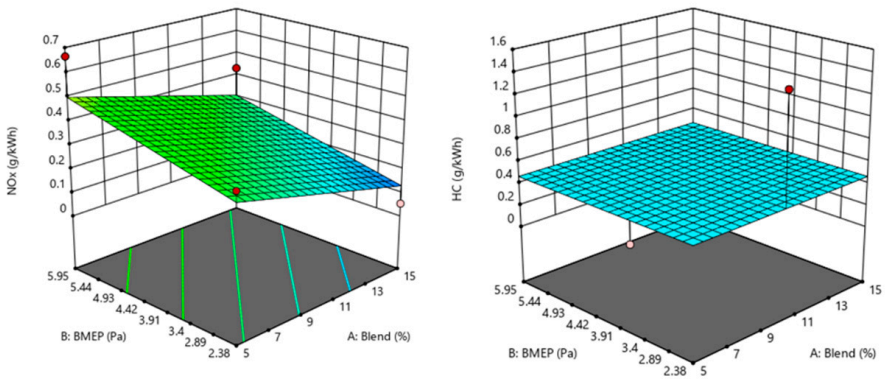


**Figure 18.** Comparative analysis of maximum $NO_x$ and HC (response to Blend-BMEP).

**Table 7.** Optimum process parameters.

| Parameter | Aim | Lower Limit | Upper Limit |
|---|---|---|---|
| δ | Within range | 2 mm | 5 mm |
| CT | Within range | 0 mm | 0.8 mm |
| E | Within range | 200 GPa | 230 GPa |
| $D_{elastic}$ | Minimize | 0.1964 mm | - |
| $\Sigma_{von\text{-}Mises}$ | Maximize | - | 872 GPa |
| $T_{surface}$ | Minimize | 315 °C | - |

**Table 8.** Optimum model validation under optimized condition.

| Sl. | Output Parameter | δ | CT | E | Predicted Value | Simulation Value | % Error |
|---|---|---|---|---|---|---|---|
| 1 | $D_{elastic}$ | 2.16 | 0.15 | 216.64 | 0.1964 mm | 0.1922 mm | 0.0042 |
| 2 | $\sigma_{von\text{-}Mises}$ | 3.79 | 0.18 | 214.64 | 872 GPa | 871.65 GPa | 0.35 |
| 3 | $T_{surface}$ | 4.27 | 0.37 | 218.16 | 315 °C | 314.1 °C | 0.9 |

## 9. Conclusions

The energy-intensive engine system upgradation and emission mitigation technique discussed here informs us that reducing the fuel carbon % through a gasoline methanol blend does not enhance carbonated emissions (CO, $CO_2$, and HC). However, $NO_x$ emissions enhanced due to an increase in the exhaust muffler temperature. Such an incremental change in heat transfer is due to the improved combustion due to the lightness of fuel. Such aggravation can be controlled through exhaust after treatment. Carbon removal up to 12% does not much alter the energy conversion process. The system energy output, fuel characteristics, and emission in the engine system is as compatible as that with the gasoline

in the energy system. In the scenario of a global energy mode swing, such an energy alternative gives hope to reforming energy policy through the emergence of methanol economy. The piston design exchange and PVD coating indirectly improve energy and efficiency by retaining a reasonable amount of heat energy. Additionally, $NO_x$ and other emission constituents were found to be under control due to piston improvement through coating. Our main conclusions observed are as follows:

- Piston type_D has a maximum CO emission of 300 gm/kWh at −8% decarbonization, while type_A and type_B have the lowest CO emission level of 50 gm/kWh at −12% decarbonization using the $B_{15}$ blend.
- At −12% decarbonization, the type_B design has the$lowestCO_2$ emission of 175 gm/kWh among all designs considered.
- For both piston designs, type_A and type_B, the $NO_x$ emission is lowest at −8% decarbonization through blending.
- Overall, it is observed that the type_A and type_B designs are more efficient compared to other designs in mitigation emission through blend replacement and design exchange.

The immediate implication of this research can be applied to newly produced automotive engines as it would not have any significant infrastructural modification. Only existing piston design modifications to type_A and type_B type would be necessary. Interfacing gasoline and methanol helps the decarbonization of power production and improves air quality. This energy innovation alternative ensures the sustainable clean energy transition. It benefits greater energy access through the inclusion of methanol as potential global energy alternatives for the ongoing energy transition to low-carbon energy resources. In addition, methanol production lies within the gasoline supply chain and its manufacturing can be aligned with petrochemical complexes that ensure almost zero additional networking. Future studies in this research may address fuel injection pressure, vaporization, and surface tension of the blend while in use.

**Supplementary Materials:** The following supporting information can be downloaded at: https://www.mdpi.com/article/10.3390/en15197188/s1, Figure S1. Emission measurement: a-Engine test bed mounted with single cylinder 4-stroke engine; b-Blend preparation; c-APPSYS E-Test Engine performance monitor; d-Emission sensor; e- Six gas emission analyzer. Figure S2. Multi piston design consideration: a. Flat head-A; b-bowl design-B; c-bowl design-C and bowl design-D. Figure S3. Structural deformation of Type-A piston design. Figure S4. Von Misses stress of thin coated Al-Si pistons at 1500 rpm and BMEP@5.95 bar. Figure S5. Von Misses stress of thick coated (0.8- and 1.2-mm CT) AlSi pistons at 1500 rpm and BMEP@5.95 bar. Figure S6. Temperature distribution of thin coated pistons at 1500 rpm and BMEP@5.95 bar. Figure S7. Temperature distribution of thick coated (0.8- and 1.2-mm CT) AlSi pistons at 1500 rpm and BMEP@5.95 bar. Table S1. Mesh convergence test for selected design. Table S2. Emission Data for Chamber-non-perforated Muffler (Pure Gasoline). Table S3. Emission Data for Chamber-non-perforated Muffler (B5, CH3OH). Table S4. Emission Data for Chamber-non-perforated Muffler (B10, CH3OH). Table S5. Emission Data for Chamber-non-perforated Muffler (B15,CH3OH). Table S6. Mesh Details for multiple designs.

**Author Contributions:** P.C.M. Conceived the study, designed the study, and wrote the paper. A.G. conducted data collection and statistical analysis. S.S. and F.K conducted simulation and data collection. R.B.I. and F.K. conducted data curation and paper writing and editing. All authors have read and agreed to the published version of the manuscript.

**Funding:** I am very much thankful to the All-India Council for Technical Education and Training (AICTE), New Delhi for funding this research. The funding of AICTE through RPS grant-in-aid to carry out our research project entitled "Advanced Engine Technology for Sustainable Development of Automotive Industry" with grant number '20/AICTE/RIFD/RPS (POLICY-III) 43/2012-13' is acknowledged. We are thankful to the computational facilities at KIIT University, and experimental facilities at the Green Engine Technology Center, School of Mechanical Engineering, KIIT University to carry out the simulation and experimental works of this research.

**Acknowledgments:** We are also thankful to our undergraduate students, Harshit Kumar Mishra and Sourav Kumar Kar and postgraduate student Abhishek Kashyap for their dedicated work in this project and their hard work on simulation and testing is acknowledged. Our collaboration with the School of

Engineering and Sustainable Development, De Montfort University, Leicester and the School of Built Environment Engineering and Computing, Leeds Beckett University in the United Kingdom is acknowledged.

**Conflicts of Interest:** The authors declare no conflict of interest.

## Abbreviations

| | |
|---|---|
| A:B,C | Independent variables |
| A/F | Air to fuel ratio |
| AlSi | Alloy of Aluminum and Silicon |
| APPSY | Measurement software for dynamometer |
| ASTM | American standard of testing and Method |
| $B_5/B_{10}/B_{15}$ | Gasoline methanol blend with 5%, 10%, and 15% methanol |
| BMEP | Break mean effective pressure |
| CO | Carbon monoxide |
| $CO_2$ | Carbon dioxide |
| CAD | Computer aided drafting |
| CT | Coating thickness |
| Delastic | Elastic deformation |
| FEA | Finite element analysis |
| FGM | Functionally graded material |
| HC | Hydrocarbon |
| HP | Horse power |
| kWh | Kilo watt hour |
| $MgZrO_3$ | Magnesium Zirconate |
| MON | Motor octane number |
| NDIR | Non-dispersive infrared |
| $NO_x$ | Nitrogen oxide |
| NiCrAl | Nickle, Chromium, and Aluminum alloy |
| $O_2$ | Oxygen |
| OCT | Octane number |
| PCI | Peripheral component interconnect |
| PVD | Physical vapor deposition |
| RON | Research octane number |
| RSM | Response surface methodology |
| $T_{surface}$ | Surface temperature |
| $\sigma_{von\text{-}Mises}$ | vonMises stress |
| $\rho$ | density |
| $\kappa$ | Kinetic viscosity |
| $\nu$ | Specific volume |

## References

1. Carley, S.; Evans, T.P.; Graff, M.; Konisky, D.M. A framework for evaluating geographic disparities in energy transition vulnerability. *Nat Energy* **2018**, *3*, 621–627. [CrossRef]
2. Grubler, A.; Wilson, C.; Bento, N.; Boza-Kiss, B.; Krey, V.; Mccollum, D.L.; Rao, N.D.; Riahi, K.; Rogelj, J.; De Stercke, S.; et al. A low energy demand scenario for meeting the 1.5 °C target and sustainable development goals without negative emission technologies. *Nat. Energy* **2018**, *3*, 515–527. [CrossRef]
3. Sgouridis, S.; Carbajales-Dale, M.; Csala, D.; Chiesa, M.; Bardi, U. Comparative net energy analysis of renewable electricity and carbon capture and storage. *Nat. Energy* **2019**, *4*, 456–465. [CrossRef]
4. Farmer, H.O. Free-piston compressor-engines. *Nature* **1947**, *159*, 413. [CrossRef]
5. He, W. The Future Development of the Internal-Combustion Engine. *Nature* **1918**, *102*, 307–308. [CrossRef]
6. Powdered Fuel: Progress and Prospects. *Nature* **1939**, *144*, 774–775. [CrossRef]
7. Markard, J. The next phase of the energy transition and its implications for research and policy. *Nat. Energy* **2018**, *3*, 628–633. [CrossRef]
8. Brockway, P.E.; Owen, A.; Brand-Correa, L.I.; Hardt, L. Estimation of global final-stage energy-return-on-investment for fossil fuels with comparison to renewable energy sources. *Nat. Energy* **2019**, *4*, 612–621. [CrossRef]
9. Raimi, D.; Carley, S.; Konisky, D. Mapping county-level vulnerability to the energy transition in US fossil fuel communities. *Sci. Rep.* **2022**, *12*, 15748. [CrossRef]

10. King, L.C.; van den Bergh, J.C.J.M. Implications of net energy-return-on-investment for a low-carbon energy transition. *Nat. Energy* **2018**, *3*, 334–340. [CrossRef]
11. Mishra, P.C.; Ishaq, R.B.; Khoshnaw, F. Mitigation Strategy of Carbon Dioxide Emissions through Multiple Muffler design exchange and Gasoline-Methanol blend replacement. *J. Clean. Prod.* **2020**, *286*, 125460. [CrossRef]
12. Mishra, P.C.; Gupta, A.; Kumar, A.; Bose, A. Methanol and petrol blended alternate fuel for future sustainable engine: A performance and emission analysis. *Measurement* **2020**, *155*, 107519, Corrigendum in *Measurement* **2022**, *199*, 111542. [CrossRef]
13. Al-Farayedhi, A.A.; Al-Dawood, A.M.; Gandhidasan, P. Effects of Blending MTBE with Unleaded Gasoline on Exhaust Emissions of SI Engine. *J. Energy Resour. Technol.* **2000**, *122*, 239–247. [CrossRef]
14. Abeydeera, L.H.U.W.; Mesthrige, J.W.; Samarasinghalage, T.I. Global Research on Carbon Emissions: A Scientometric Review. *Sustainability* **2019**, *11*, 3972. [CrossRef]
15. Anenberg, S.; Miller, J.; Minjares, R.; Du, L.; Henze, D.K.; Lacey, F.; Malley, C.S.; Emberson, L.; Franco, V.; Klimont, Z.; et al. Impacts and mitigation of excess diesel-related NOx emissions in 11 major vehicle markets. *Nature* **2017**, *545*, 467–471. [CrossRef] [PubMed]
16. Verhelst, S.; Turner, J.W.; Sileghem, L.; Vancoillie, J. Methanol as a fuel for internal combustion engines. *Prog. Energy Combust. Sci.* **2019**, *70*, 43–88. [CrossRef]
17. Yao, Y.; Chang, Y.; Huang, R.; Zhang, L.; Masanet, E. Environmental implications of the methanol economy in China: Well-to-wheel comparison of energy and environmental emissions for different methanol fuel production pathways. *J. Clean. Prod.* **2018**, *172*, 1381–1390. [CrossRef]
18. Riaz, A.; Zahedi, G.; Klemeš, J.J. A review of cleaner production methods for the manufacture of methanol. *J. Clean. Prod.* **2013**, *57*, 19–37. [CrossRef]
19. Nguyen, T.B.; Zondervan, E. Methanol production from captured $CO_2$ using hydrogenation and reforming technologies_ environmental and economic evaluation. *J. CO2 Util.* **2019**, *34*, 1–11. [CrossRef]
20. Masum, B.; Masjuki, H.; Kalam, M.; Palash, S.; Habibullah, M. Effect of alcohol–gasoline blends optimization on fuel properties, performance and emissions of a SI engine. *J. Clean. Prod.* **2015**, *86*, 230–237. [CrossRef]
21. Wang, Y.; Lin, L.; Roskilly, A.P.; Zeng, S.; Huang, J.; He, Y.; Huang, X.; Huang, H.; Wei, H.; Li, S.; et al. An analytic study of applying Miller cycle to reduce NOx emission from petrol engine. *Appl. Therm. Eng.* **2007**, *27*, 1779–1789. [CrossRef]
22. Mishra, P.C.; Kar, S.K.; Mishra, H. Effect of perforation on exhaust performance of a turbo pipe type muffler using methanol and gasoline blended fuel: A step to NOx control. *J. Clean. Prod.* **2018**, *183*, 869–879. [CrossRef]
23. Baker, R.A., Sr.; Doerr, R.C. Catalytic Reduction of Nitrogen Oxides in Automobile Exhaust. *J. Air Pollut. Control Assoc.* **1964**, *14*, 409–414. [CrossRef] [PubMed]
24. Esfahanian, V.; Javaheri, A.; Ghaffarpour, M. Thermal analysis of an SI engine piston using different combustion boundary condition treatments. *Appl. Therm. Eng.* **2006**, *26*, 277–287. [CrossRef]
25. Liu, Y.; Reitz, R.D. *Multidimensional Modelling of Combustion Chamber Surface Temperatures*; SAE Technical Paper 971593; SAE: Warrendale, PA, USA, 1997. [CrossRef]
26. Buyukkaya, E. Thermal analysis of functionally graded coating AlSi alloy and steel pistons. *Surf. Coatings Technol.* **2008**, *202*, 3856–3865. [CrossRef]
27. Taymaz, I.; Çakır, K.; Mimaroglu, A. Experimental study of effective efficiency in a ceramic coated diesel engine. *Surf. Coatings Technol.* **2005**, *200*, 1182–1185. [CrossRef]
28. Taymaz, I. The effect of thermal barrier coatings on diesel engine performance. *Surf. Coatings Technol.* **2007**, *201*, 5249–5252. [CrossRef]
29. Buyukkaya, E.; Cerit, M. Thermal analysis of a ceramic coating diesel engine piston using 3-D finite element method. *Surf. Coatings Technol.* **2007**, *202*, 398–402. [CrossRef]
30. Yessian, S.; Varthanan, P.A. Optimization of Performance and Emission Characteristics of Catalytic Coated IC Engine with Biodiesel Using Grey-Taguchi Method. *Sci. Rep.* **2020**, *10*, 2129. [CrossRef]
31. Verma, P.; Zare, A.; Jafari, M.; Bodisco, T.; Rainey, T.; Ristovski, Z.; Brown, R.J. Diesel engine performance and emissions with fuels derived from waste tyres. *Sci. Rep.* **2018**, *8*, 2457. [CrossRef]
32. Ordouei, M.H.; Elkamel, A.; Dusseault, M.B.; Alhajri, I. New sustainability indices for product design employing environmental impact and risk reduction: Case study on gasoline blends. *J. Clean. Prod.* **2015**, *108*, 312–320. [CrossRef]
33. Ou, S.; He, X.; Ji, W.; Chen, W.; Sui, L.; Gan, Y.; Lu, Z.; Lin, Z.; Deng, S.; Przesmitzki, S.; et al. Machine learning model to project the impact of COVID-19 on US motor gasoline demand. *Nat. Energy* **2020**, *5*, 666–673. [CrossRef]
34. Zhou, N.; Khanna, N.; Feng, W.; Ke, J.; Levine, M. Scenarios of energy efficiency and $CO_2$ emissions reduction potential in the buildings sector in China to year 2050. *Nat. Energy* **2018**, *3*, 978–984. [CrossRef]
35. Figueredo, A.J.; Wolf, P.S. Assortative pairing and life history strategy—A cross-cultural study. *Hum. Nat.* **2009**, *20*, 317–330. [CrossRef]
36. Hao, Z.; AghaKouchak, A.; Nakhjiri, N.; Farahmand, A. Global integrated drought monitoring and prediction system (GIDMaPS) data sets. *Figshare* **2014**, *1*, 140001. [CrossRef]
37. Montgomery, D.C. Design and Analysis of Experiments. *J. Am. Stat. Assoc.* **2000**, *16*, 2.

38. Wang, X.; Chen, H.; Liu, H.; Li, P.; Yan, Z.; Huang, C.; Zhao, Z.; Gu, Y. Simulation and optimization of continuous laser transmission welding between PET and titanium through FEM, RSM, GA and experiments. *Opt. Lasers Eng.* **2013**, *51*, 1245–1254. [CrossRef]
39. Zhang, Z.; Tian, J.; Xie, G.; Li, J.; Xu, W.; Jiang, F.; Huang, Y.; Tan, D. Investigation on the combustion and emission characteristics of diesel engine fueled with diesel/methanol/n-butanol blends. *Fuel* **2022**, *314*, 123088. [CrossRef]
40. Zhang, Z.; Li, J.; Tian, J.; Dong, R.; Zou, Z.; Gao, S.; Tan, D. Performance, combustion and emission characteristics investigations on a diesel engine fueled with diesel/ethanol/n-butanol blends. *Energy* **2022**, *249*, 123733. [CrossRef]